

# OIM in practice

**K. Sztwiertnia**

*Polish Academy of Sciences, Institute of Metallurgy and Materials  
Science, 25 Reymonta St., 30-059 Krakow, Poland*



# Contents

Example I: *In situ* TEM observation of the recrystallization in fcc alloys with low stacking fault energies.

Example II: Recrystallization of aluminium alloy with bimodal second-phase particle distribution.

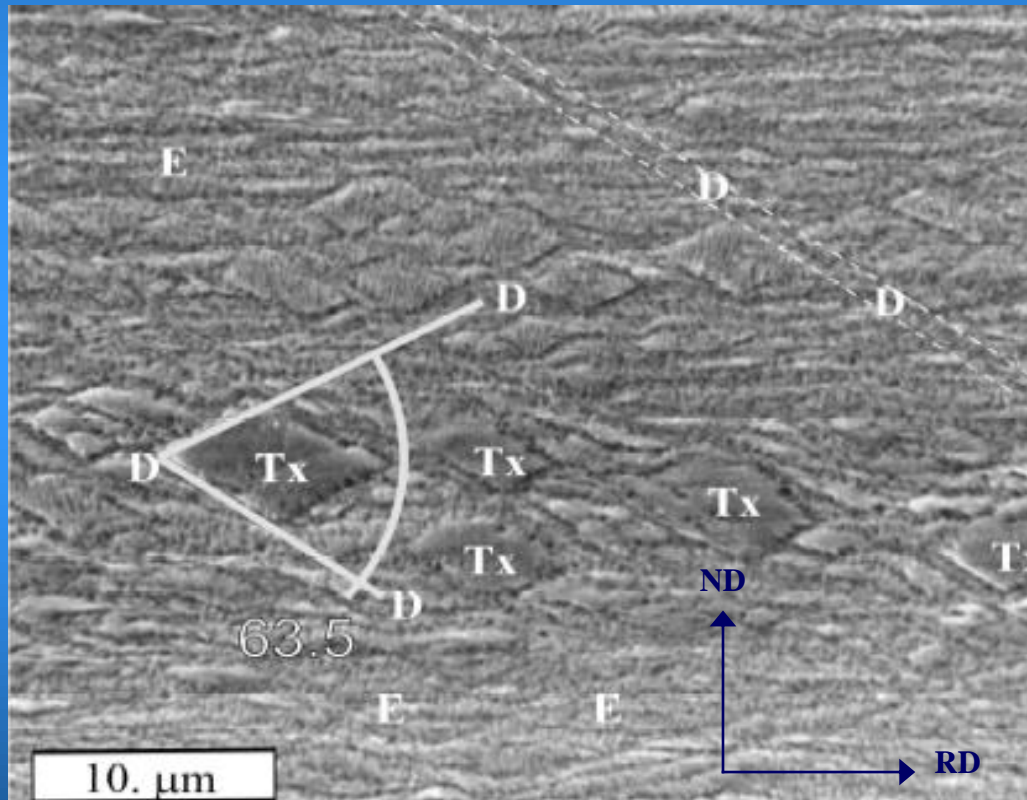
Example III: Gradient microstructure of Fe-Cr-Co alloys subjected to complex load.

Example IV: Orientation mapping applied to composites.



# Example I: *In situ* TEM observation of the recrystallization in fcc alloys with low stacking fault energies.

## As-deformed microstructure of 95% cold-rolled CuZn28, SEM.



$$\gamma_{SFE} < 25 \text{ mJm}^{-2}$$

### Deformation Stage

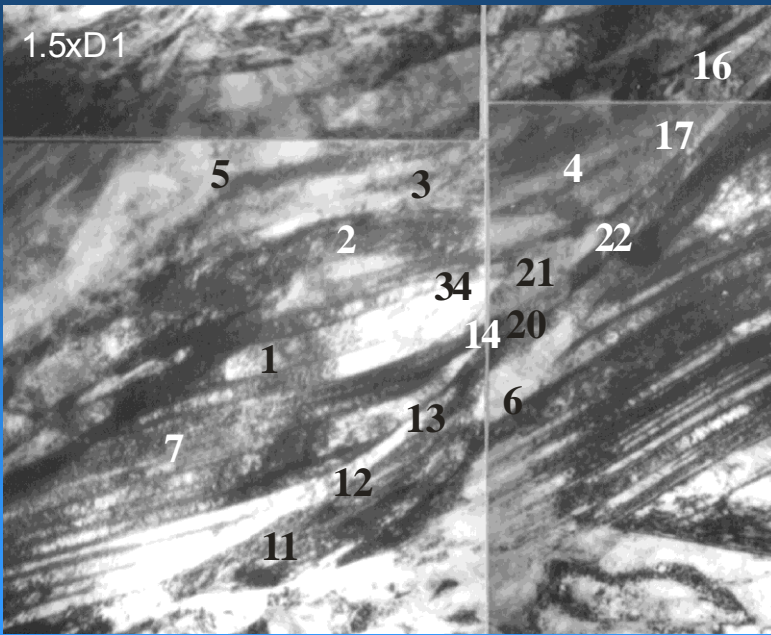
#### The brass-type texture with the components:

- Brass={011}<211>,
- S={213}<364>,
- Goss={011}<100>.

#### Microstructure:

- wavy layers of microbands (E),
- rhombic domains built of „bundles,, consisting of deformation-twin lamellae and fragments of a non-twined matrix (Tx),
- shear bands (D).



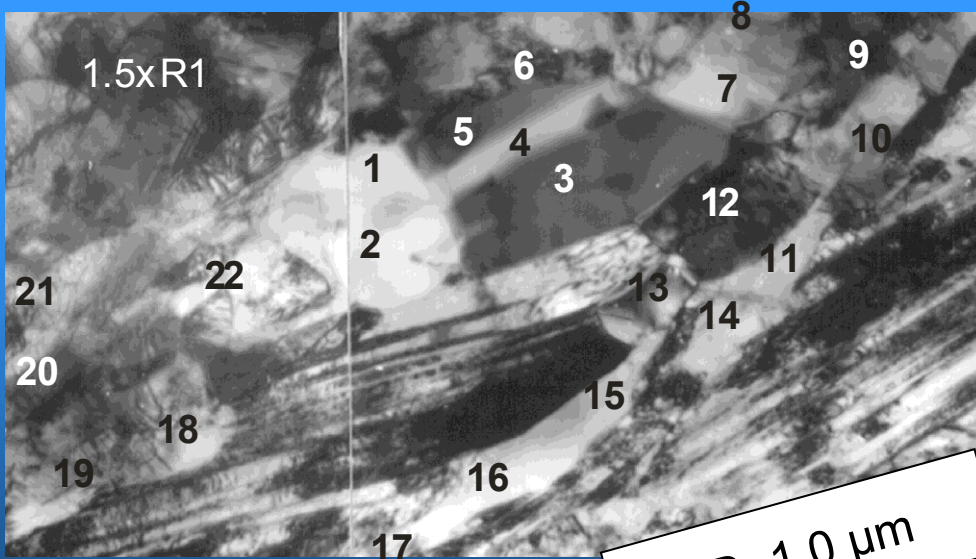


3 360. 39. 37. Brass\_30TD3(8.5)  
 Microstructure of 95% cold rolled  
 CuP1, as observed before and after  
 heating in a longitudinal section by  
 the TEM

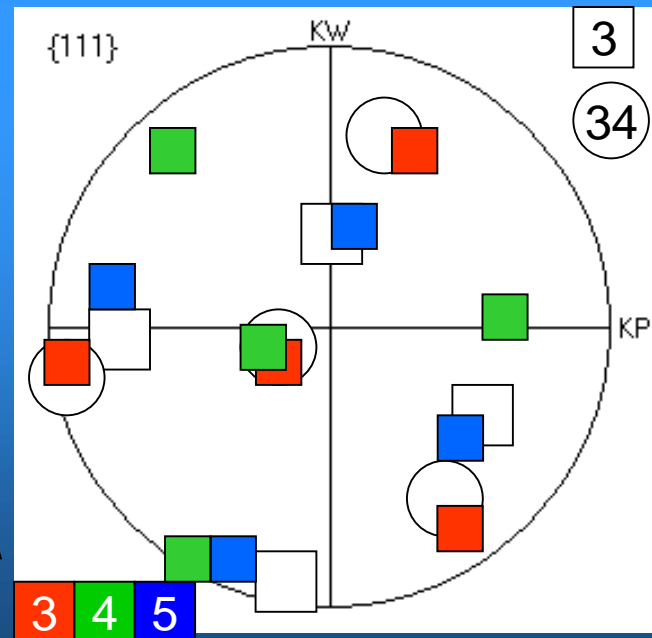
<< 1 34.7 [114](2.0)S33  
 << 34 2.7 [577](1.4)  
 << 284.49.61. R\_Brass\_9(12.3)  
 << 1 45.8 [335](2.4)

5 127. 29. 29. S \_\_\_\_\_ 4(11.1)  
 << 3 9.6 [155](2.4)

<< 4 53.3 [122](2.7)S45

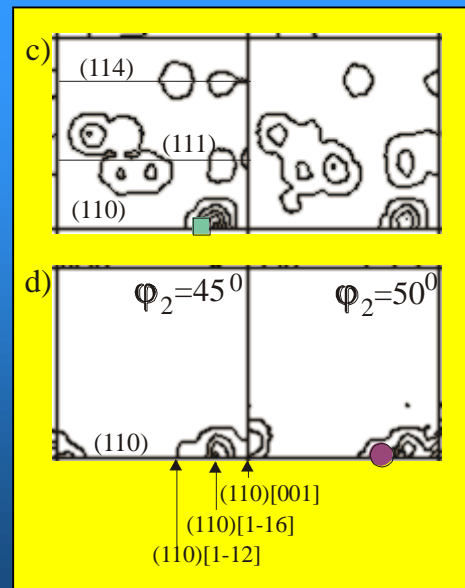
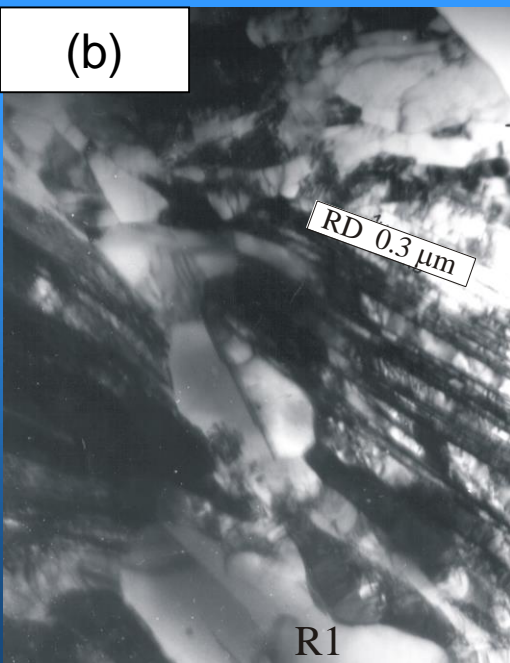
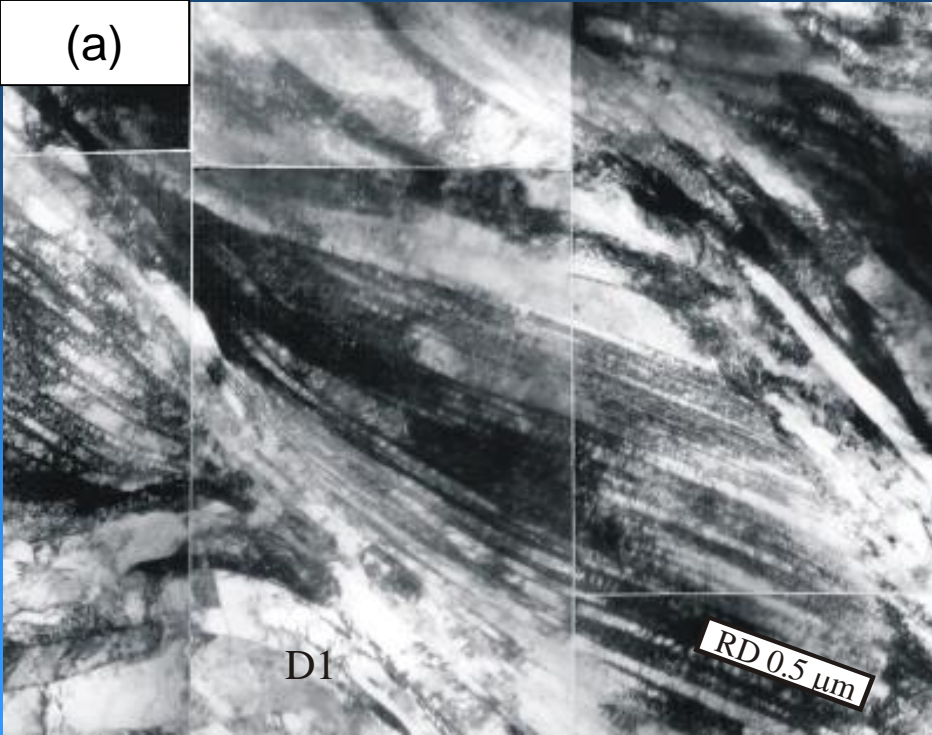


RD 1.0  $\mu$ m

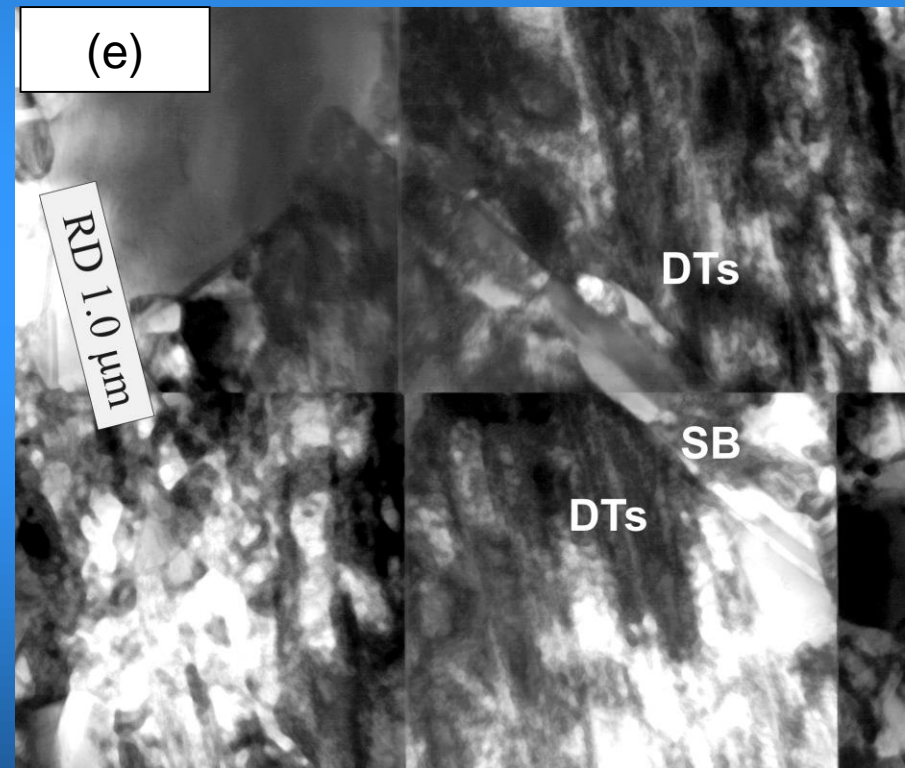


K. Sztwiertnia



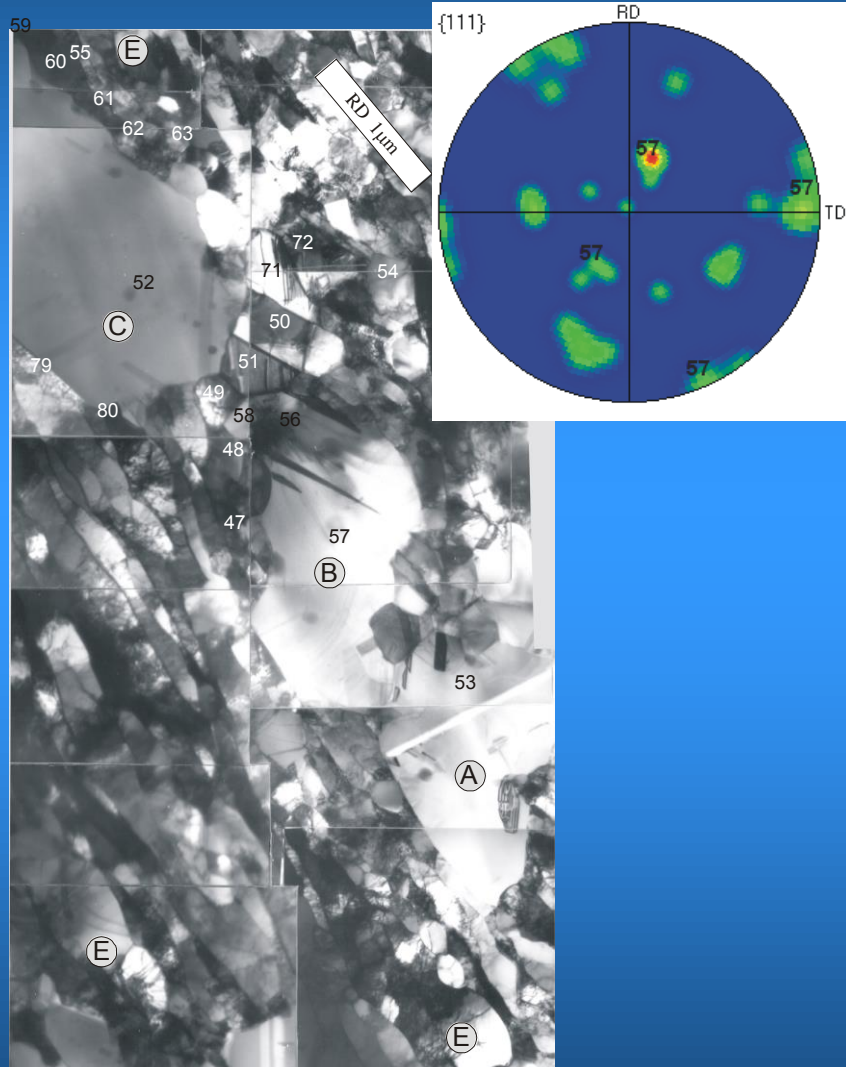
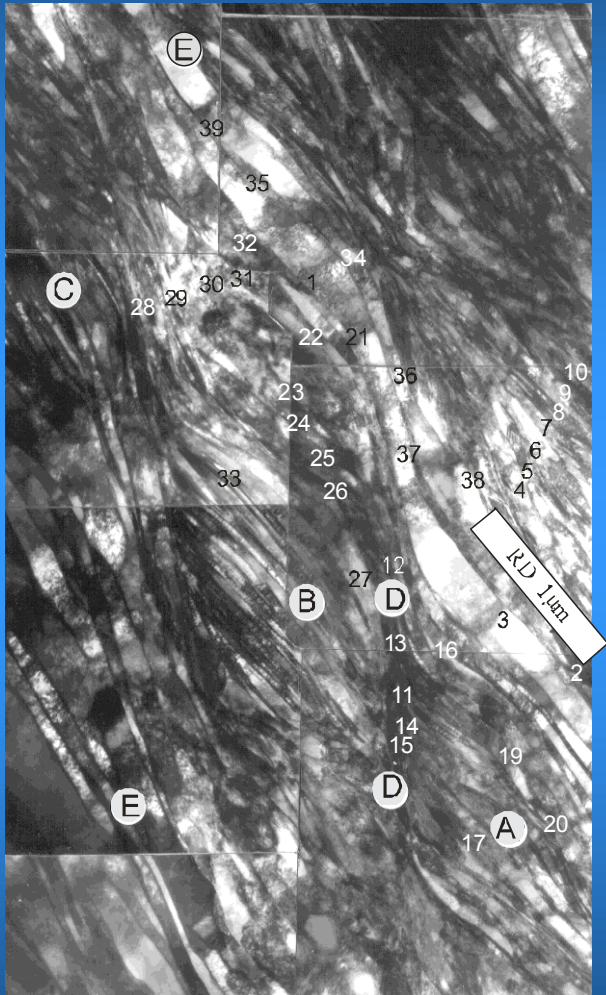


**a and b** - Microstructure of 95% cold rolled CuP1, as observed before and after heating;  
**e** - the microstructure of CuZn28 95% cold-rolled and subsequently heated in the calorimeter to 240 °C, a longitudinal section, TEM.

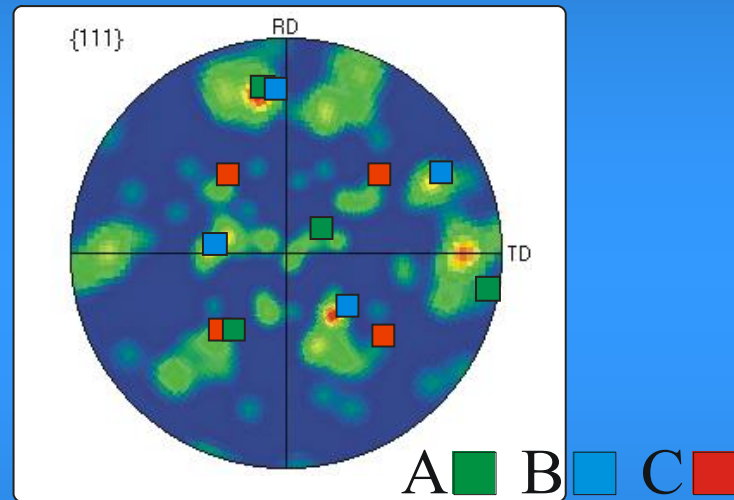
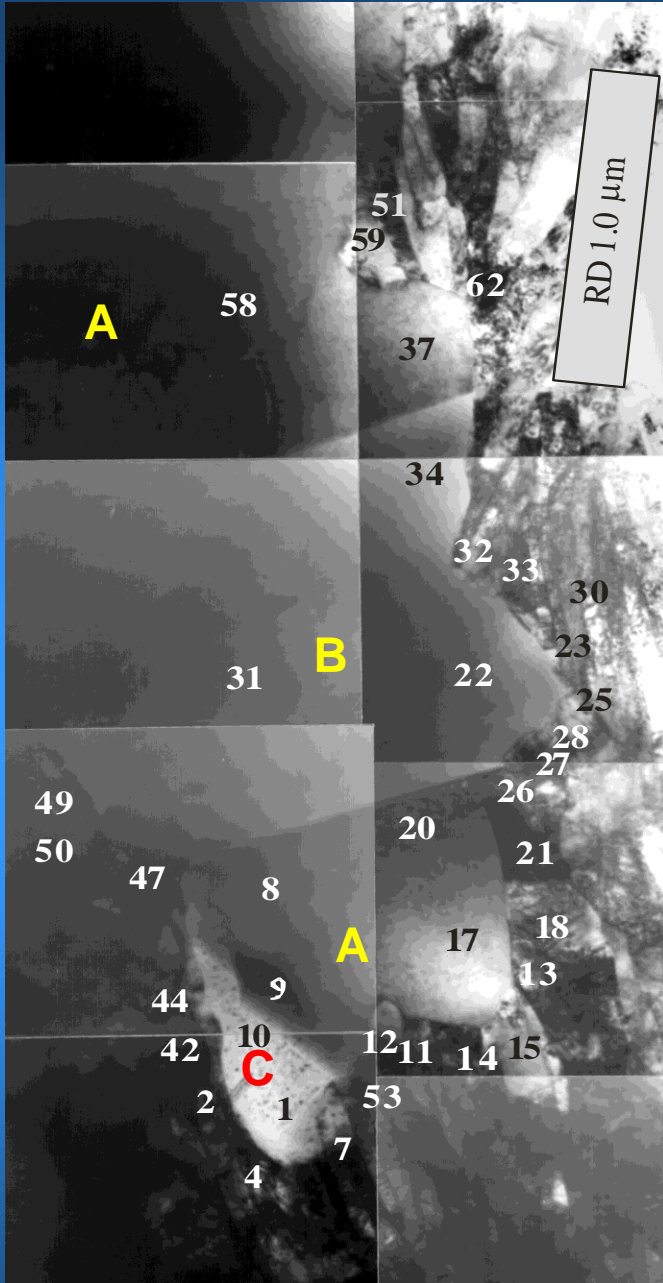


**K. Sztwiertnia:** On recrystallization texture formation in polycrystalline fcc alloys with low stacking fault energies, *Int. J. Mater. Res.*, 99 (2008) 178 – 190.

# Microstructure of 95% cold rolled CuP1, as observed before and after heating in a longitudinal section by the TEM.



Microstructure of 90% cold rolled silver, as observed after heating in the calorimeter to 90 °C, a longitudinal section, TEM.



A=37 205. 42. 30. S\_\_\_M15TD1(11.8)

B=22 297. 25. 90. R\_Brass\_\_\_2(18.7)

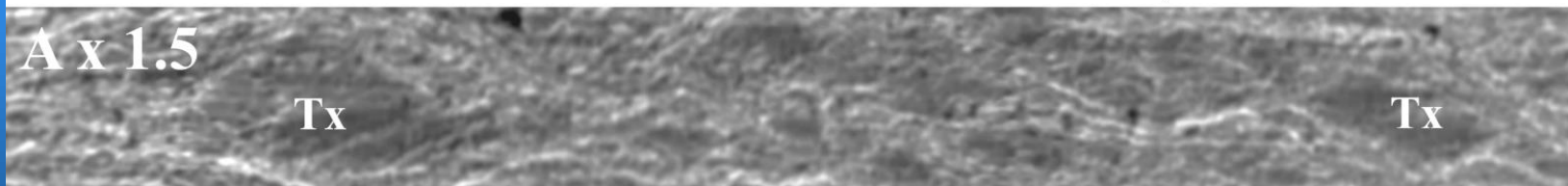
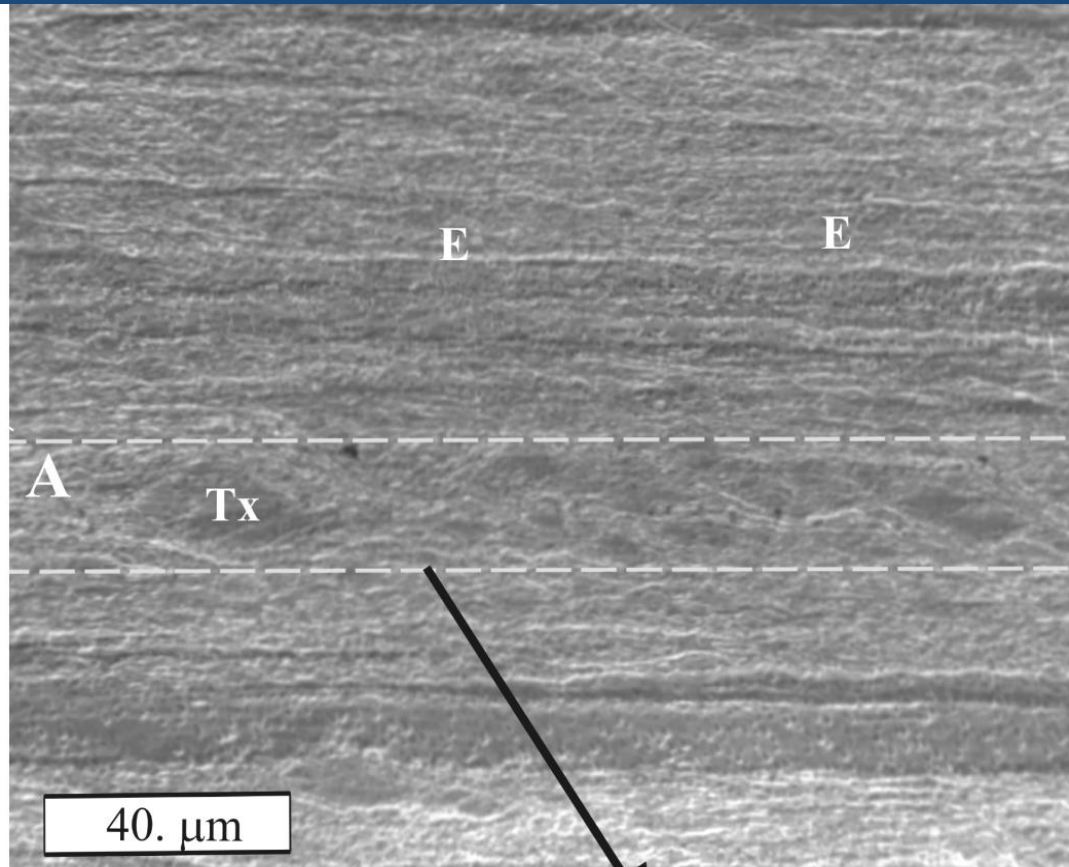
A= 9 205. 41. 30. S\_\_\_M15TD1(11.9)

C= 1 48. 8. 42. Cube\_\_\_\_\_3( 7.6)





**As-deformed  
microstructure  
of 90% cold-  
rolled silver,  
SEM.**

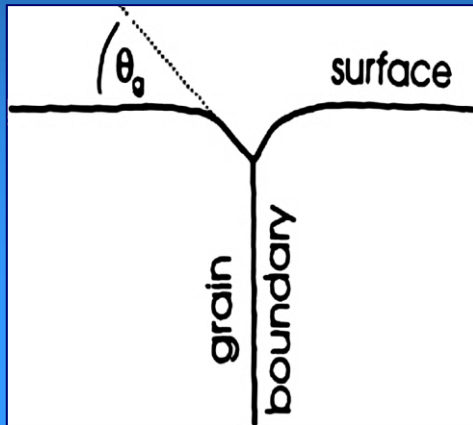


K. Sztwiertnia

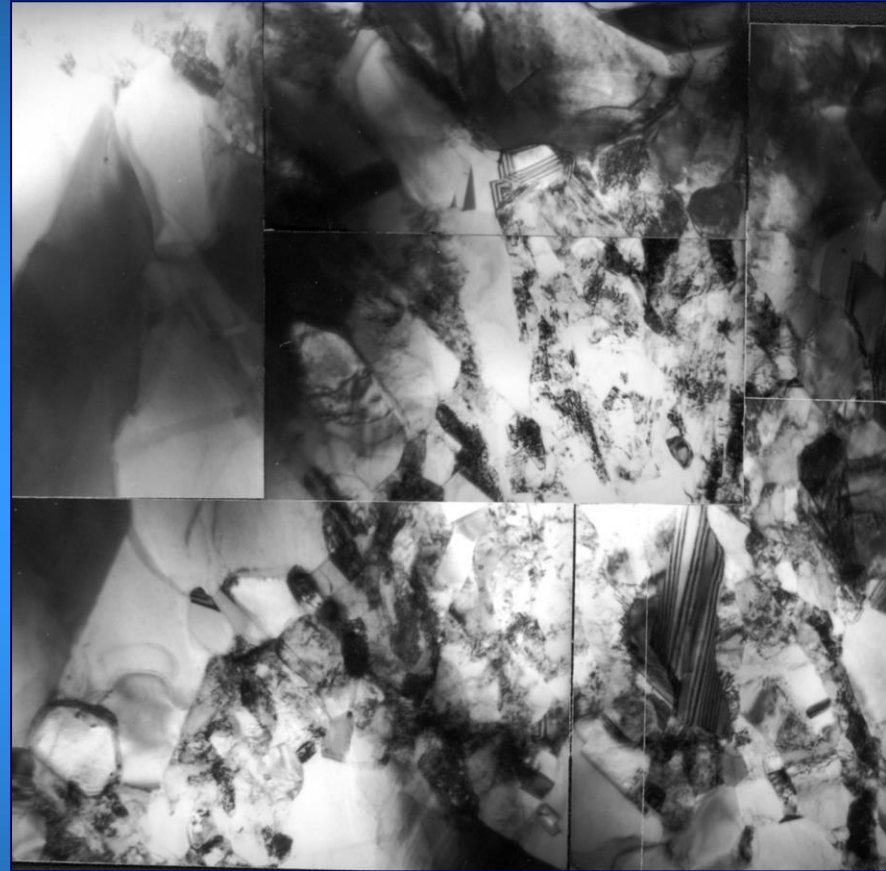
**K. Sztwiertnia:** *On recrystallization texture formation in polycrystalline fcc alloys with low stacking fault energies,* International Journal of Materials Research, 99 (2008) 178 – 190.



# Microstructure of 95% cold-rolled CuZn28 as observed after heating in the TEM, a longitudinal section.



Thermal grooving at the surface.



K. Sztwiertnia, M. Bieda, G. Sawina: Polska Metalurgia w latach 2002-2006, red. wyd. K. Świątkowski, Komitet Metalurgii Polskiej Akademii Nauk, (2006) 747-752.

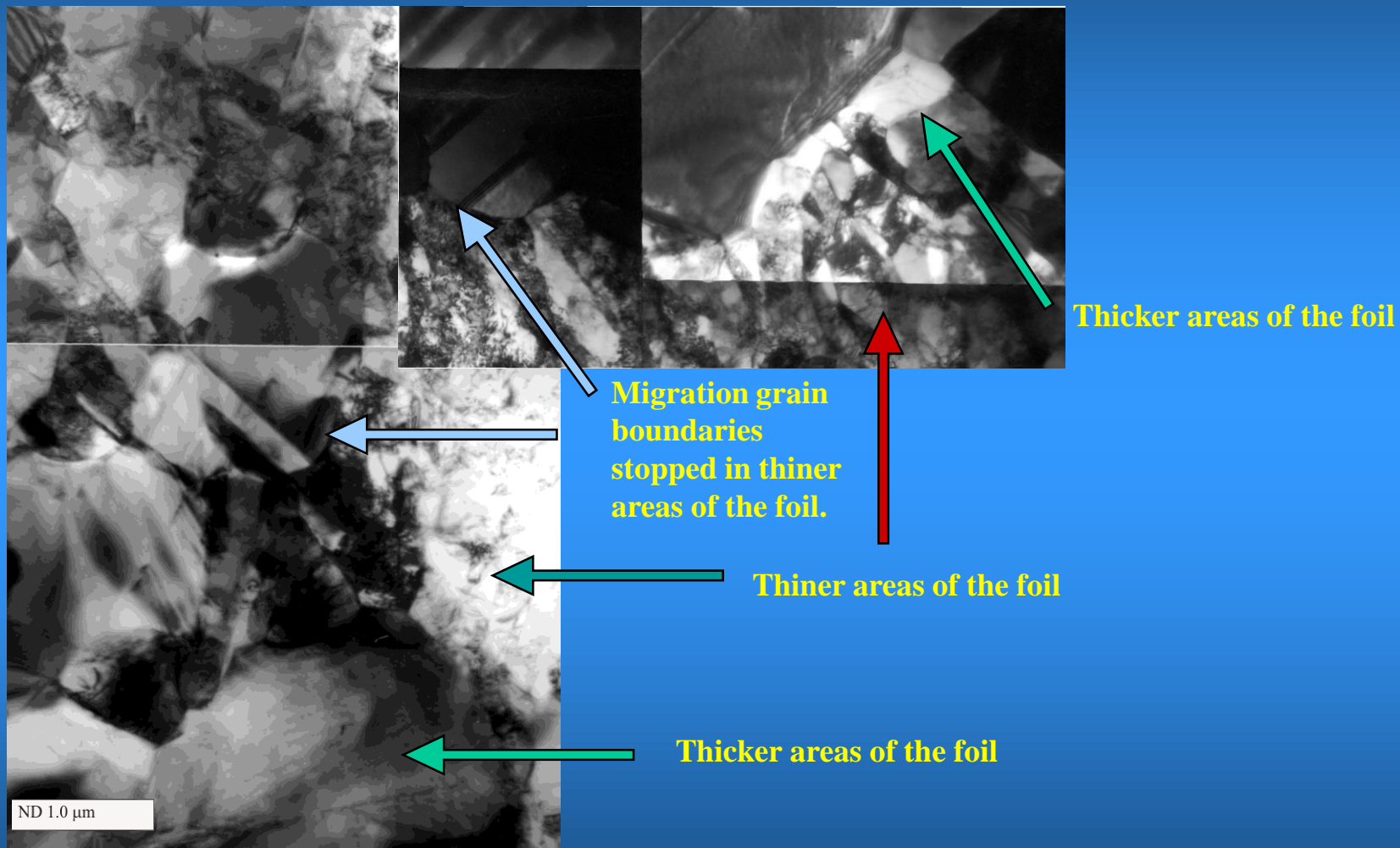


K. Sztwiertnia

W.W. Mullins: Acta metall., 6 (1958) 414.

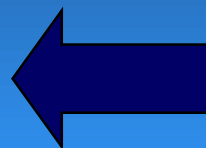
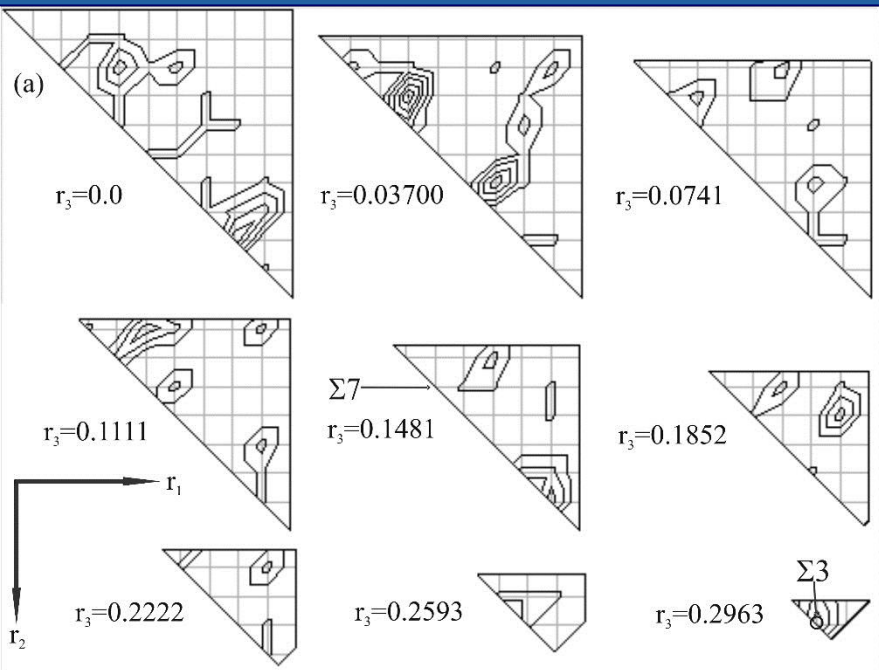
W. Roberts, B. Lehtinen: Phil. Mag., 26 (1972) 1153.

# Microstructure of 95% cold-rolled CuZn28 as observed after heating in the TEM, a longitudinal section.



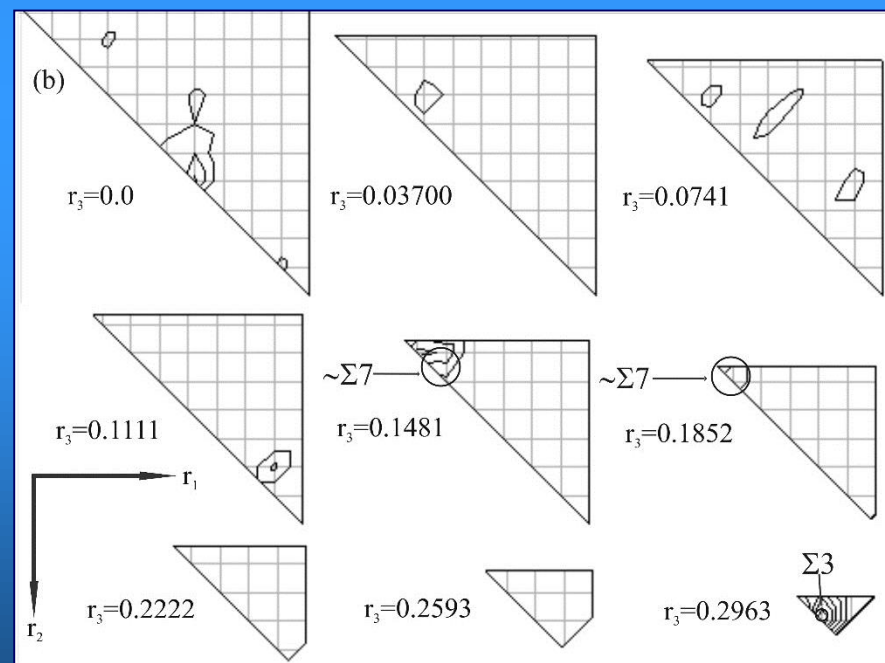
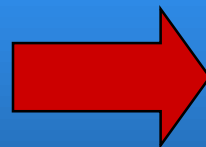
# Misorientation Distribution Functions of Recrystallization Fronts

Rodrigues' representation  $r_1, r_2, r_3$ , cross-section  $r_3 = \text{const.}$ , asymmetric domain (O, O).  
(High angle grain boundaries only;  $\omega > 15^\circ$ ).

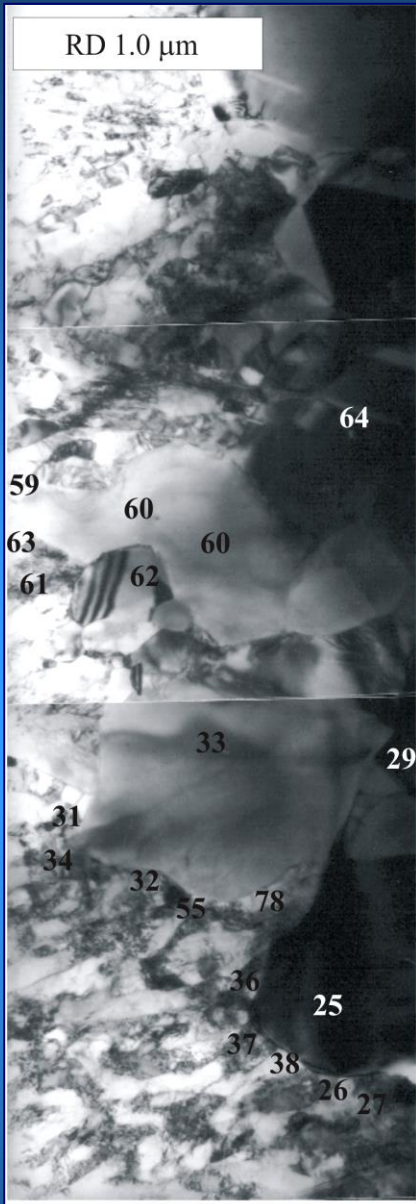


MDF for recrystallization fronts in bulk, partly recrystallized samples; 122 misorientations.

MDF for recrystallization fronts stopped in thinner regions of the foils; 264 misorientations.



K. Sztwiertnia



Nr1	$\phi_1$	$\Phi$	$\phi_2$	texture component
>>Nr2	$\omega$	[uvw]	( $\alpha$ )	
26	353.	45.	53.	Brass_30TD3(11.3)
27	352.	45.	54.	Brass_30TD3(11.7)
29	313.	41.	21.	S_____3( 9.6)
31	353.	45.	55.	Brass_30TD3(11.5)
32	263.	21.	82.	T2_111_1101(12.5)
34	353.	45.	55.	Brass_30TD3(11.5)
36	353.	45.	54.	Brass_30TD3(11.4)
37	265.	21.	80.	T2_111_1101(11.9)
38	293.	44.	38.	S_____M15TD3( 5.8)
55	313.	41.	21.	S_____3( 9.6)
59	321.	38.	18.	T1_S_____2(12.1)
61	176.	31.	81.	ND-Goss___3(14.9)
62	210.	48.	27.	T1_Cube___1( 3.7)
63	174.	31.	84.	ND-Goss___3(14.3)
64	288.	28.	14.	T2_R_Brass4(13.9)
25	41.	30.	88.	S_____P15TD1( 6.8)
>>	27	-36.4	[012]	( 0.8)
>>	26	-35.8	[012]	( 0.2)
<<	29	59.9	[111]	( 0.1) $\Sigma$ 3
<<	38	54.5	[335]	( 2.9)
<<	37	54.4	[557]	( 1.4)
>>	36	-36.0	[012]	( 0.7)
33	270.	38.	32.	R_Brass___2(11.9)
>>	55	-35.9	[355]	( 1.0)
<<	34	38.2	[001]	( 5.5) $\Sigma$ 5
>>	32	-48.1	[114]	( 2.6)
<<	31	38.2	[001]	( 5.5) $\Sigma$ 5
<<	78	19.8	[113]	( 1.0)
60	209.	48.	27.	T1_Cube___1( 3.4)
<<	59	40.3	[577]	( 2.5) $\Sigma$ 7
<<	61	37.9	[011]	( 1.3) $\Sigma$ 9
<<	63	39.5	[011]	( 0.7) $\Sigma$ 9
>>	62	-0.6	[235]	( 5.1)
<<	64	59.5	[111]	( 1.3) $\Sigma$ 3

Recrystallization front stopped in thinner regions of the foil.

Orientations are given in Euler's angles  $\phi_1$ ,  $\Phi$ ,  $\phi_2$ . Letters with numbers indicate the sample symmetry related variants of the components nearest to the measured orientations (the numbers in brackets give the angle of disorientation  $\omega_{min}$  from the particular component).

Misorientations are given by the angle of disorientation  $\omega_d$  and rotation axis [uvw].





## CONCLUSIONS

- TEM measurements are suitable for the *in situ* study of localized strain regions (interesting as nucleation sites).
- The proximity of the free surface in thin foils can be a complicated factor during annealing. However, the experimental conditions can be determined, which ensure that the changes directly observed in an annealed foil are at least close to those occurring in a bulk sample.
- Due to thermal grooving, the recrystallization front always stops in the foil thinner than a certain critical value, which approximately depends on the fineness of its microstructure.
- The distributions of misorientations along the recrystallization fronts stopped in thin areas of foils during the *in situ* measurements are (probably) “more real”, than the distributions measured in “frozen” bulk samples.



**Example II:** Recrystallization of aluminium alloy with bimodal second-phase particle distribution.

## Recrystallization of 6013 aluminium alloy

Alloy 6013, chemical composition (% by weight).

Mg	Si	Cu	Mn	Fe	Others	Al
1.15	1.0	1.1	0.3	0.5	0.15	Remainder



The material for testing was supersaturated (kept for 1 hour at the temperature of  $530^{\circ}\text{C}$ ), then aged at the temperature of  $165^{\circ}\text{C}$  for 5 days. In this way, a relatively uniform distribution of stable, second-phase particles, both small ( $\ll 1\mu\text{m}$ ) and large ( $>1\mu\text{m}$ ) ones, was obtained. Aged samples were 75% reversible cold-rolled and then annealed in a calorimeter to achieve defined stages of recrystallization.

The investigations:

- Measurements of local crystallographic orientations in the TEM;
  - in a state after deformation,
  - after heating in the TEM.
- Calorimetric measurements of recrystallization (non-isothermal method, differential calorimeter).
- Analysis of microstructures and local orientation distributions in samples annealed in a calorimeter to the various recrystallization stages.



# The state after deformation - commercially pure aluminum (3N Al)

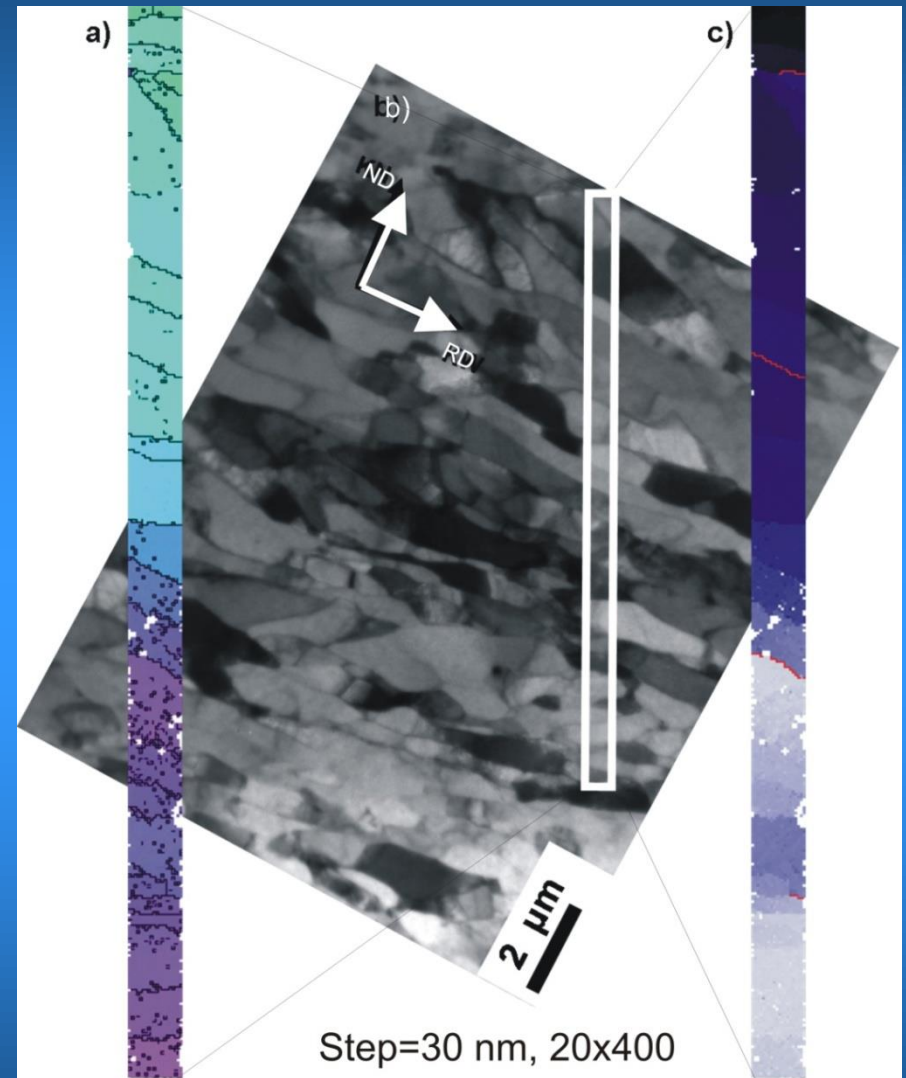
Example of microstructure of 90% cold-rolled aluminum; (b) the TEM bright field image, (a and c) orientation topographies.

On the map (c) the color change indicates a deviation from the initial orientation (dark blue) to the disoriented orientation (light blue);

(a) black lines - low angle grain boundaries ( $>1^\circ$ );

(c) red lines - the boundaries with a disorientation angle  $> 5^\circ$ ;

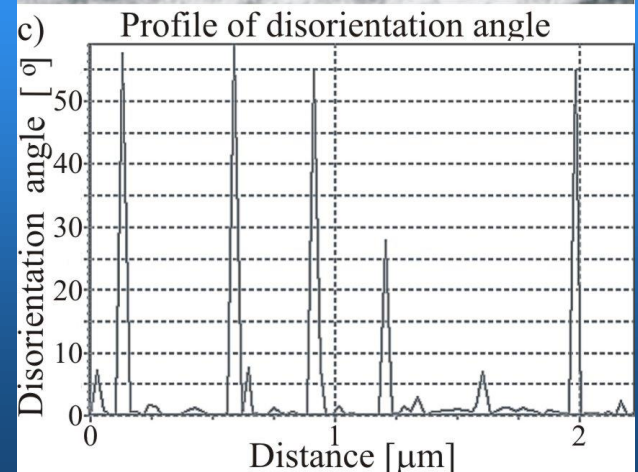
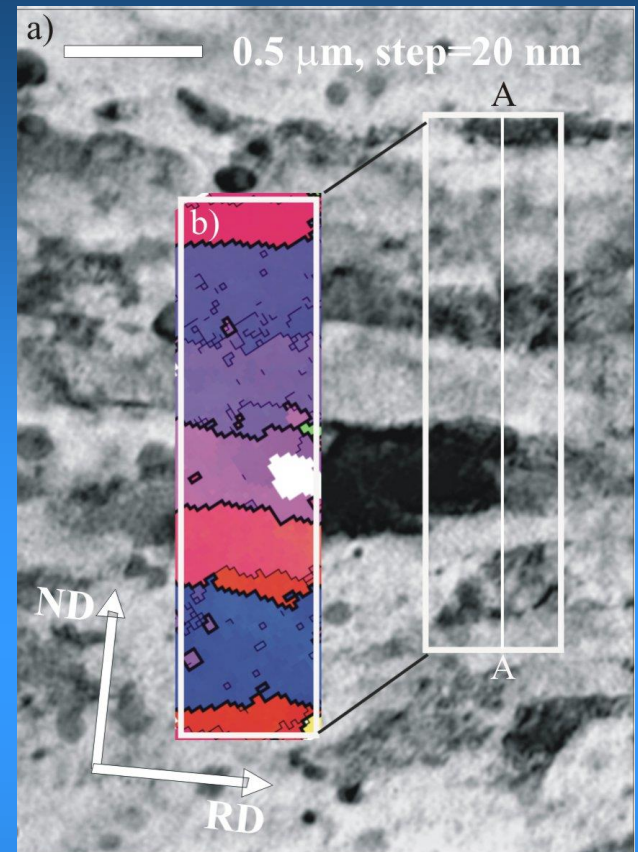
the points where the diffraction pattern has not been solved are shown in white.





# The state after deformation - 6013 aluminum alloy

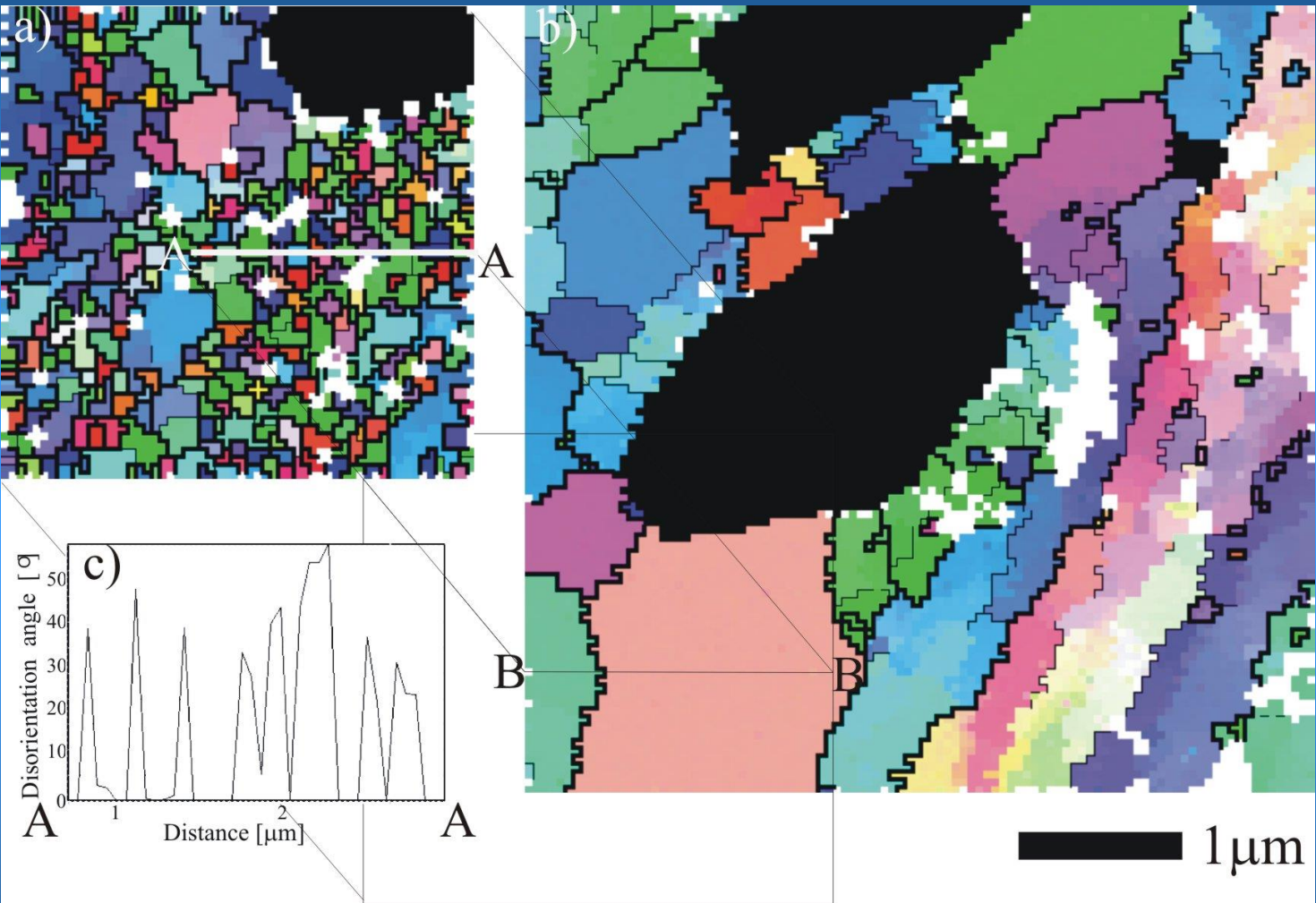
- a) Example of microstructure of 75% cold-rolled 6013 alloy, longitudinal section, TEM.
- b) Orientation topography of the matrix area, thick lines – HAGBs, thin lines – LAGBs; white regions – not indexed.
- c) Disorientation angle profile along A–A line (b)



The HAGBs length in the cold-rolled up to 90% samples reached a value of about  $100 \mu\text{m}/\mu\text{m}^2$  in areas adjacent to the large second-phase particles and about  $40 \mu\text{m}/\mu\text{m}^2$  in the matrix.

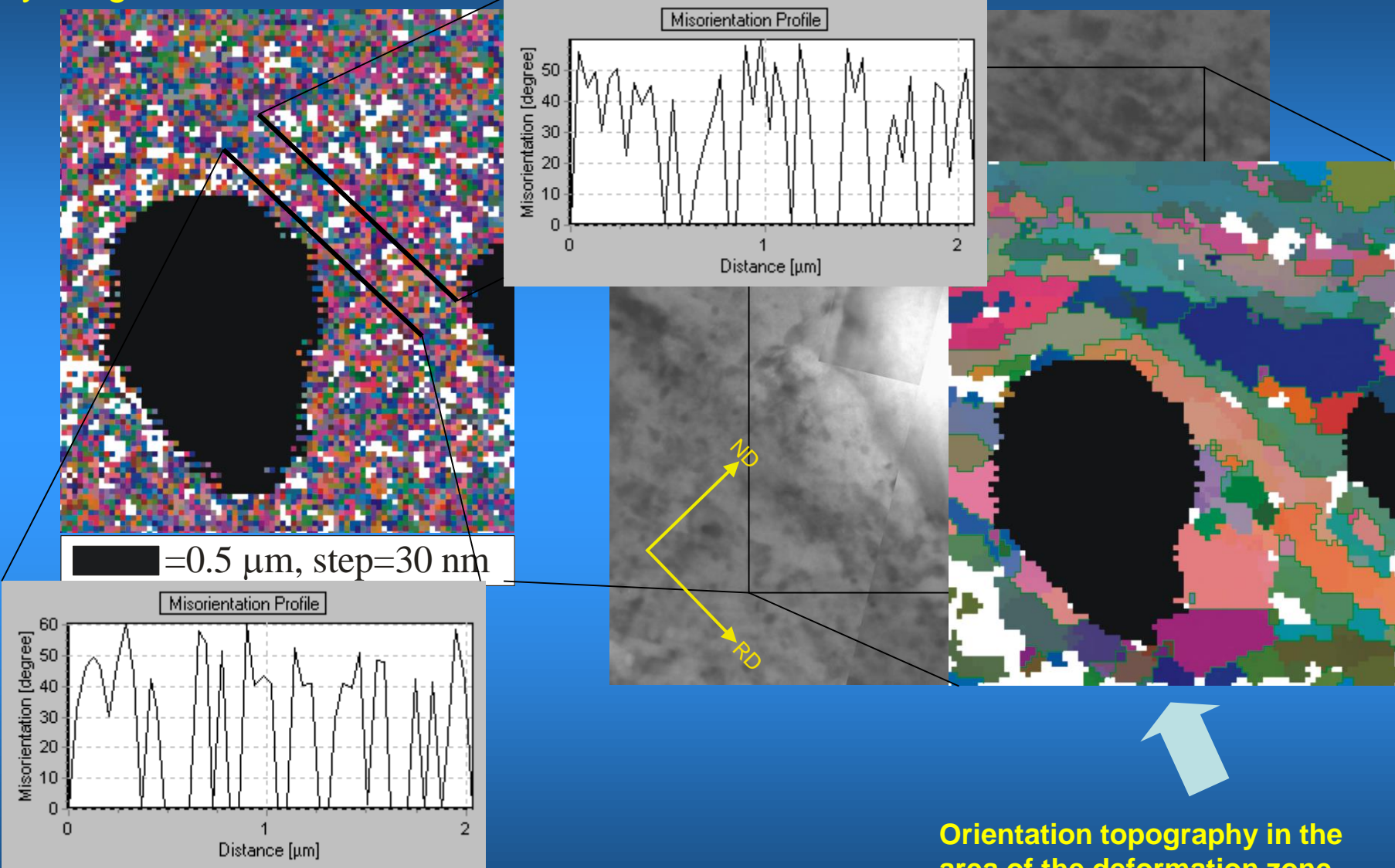


Example of orientation topography in an area of the deformation zone around the large particles (a) before and (b) after annealing *in situ* in TEM; 75% cold-rolled 6013 aluminum alloy, longitudinal section, TEM.



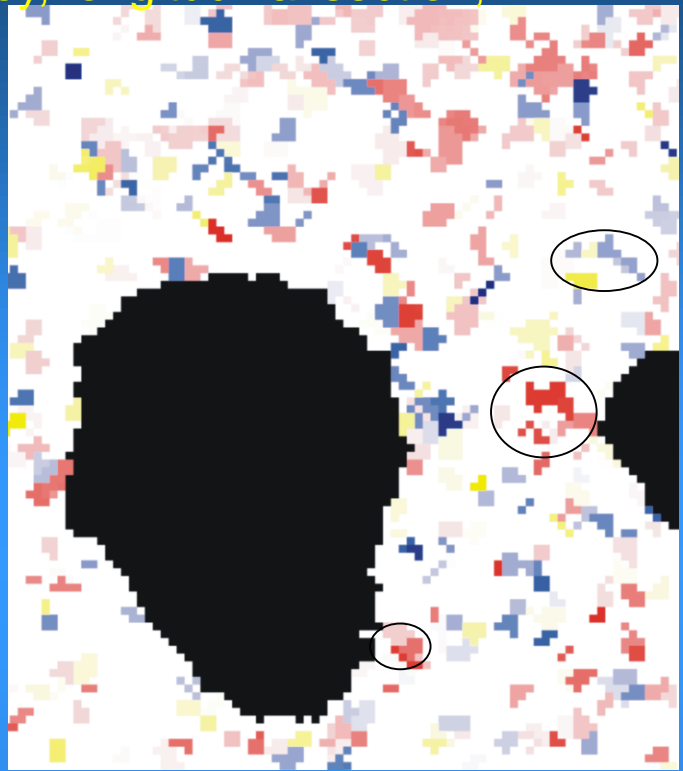
Particles of the second phase – black, white regions – not indexed; thick lines – HAGBs, thin lines – LAGBs; longitudinal section, TEM. d) Example of disorientation angle profile along A-A.

Example of orientation topography in an area of the deformation zone around the large particles before and after annealing *in situ* in TEM; 90% cold-rolled 6013 aluminum alloy, longitudinal section, TEM.



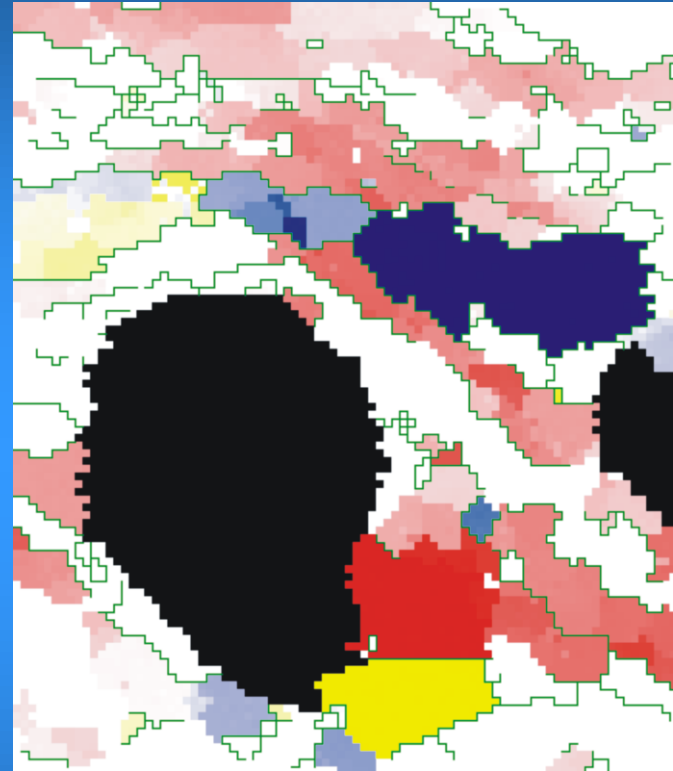
Orientation topography in the area of the deformation zone after heating *in-situ* in TEM

Example of orientation topography in an area of the deformation zone around the large particles before and after annealing *in situ* in TEM; 90% cold-rolled 6013 aluminum alloy, longitudinal section, TEM.

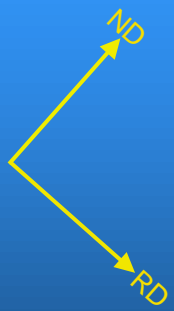


■ = 0.5  $\mu\text{m}$ , step = 30 nm

Orientation topography in the area of the deformation zone



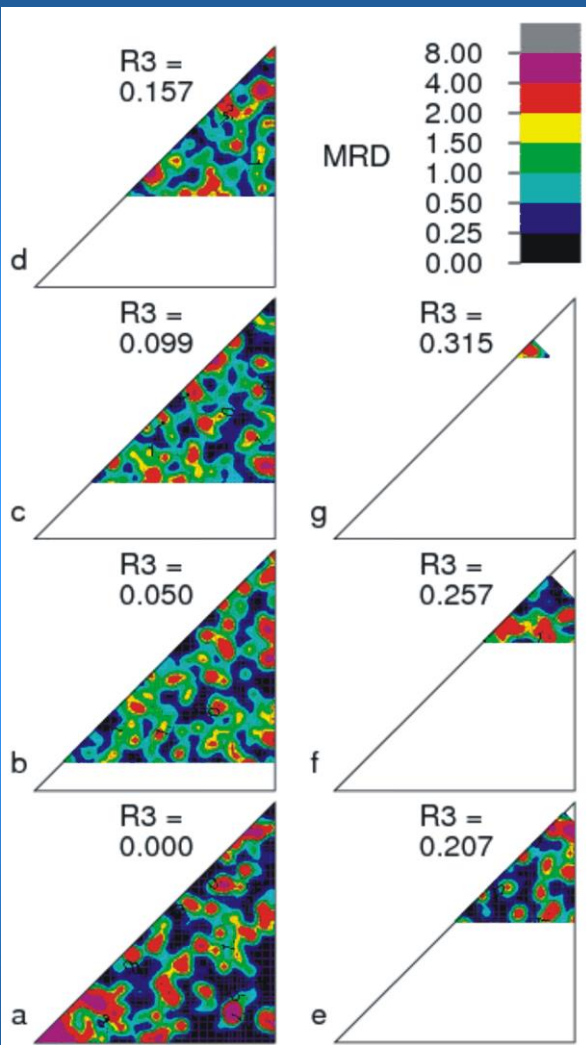
Orientation topography in the area of the deformation zone after heating *in-situ* in TEM





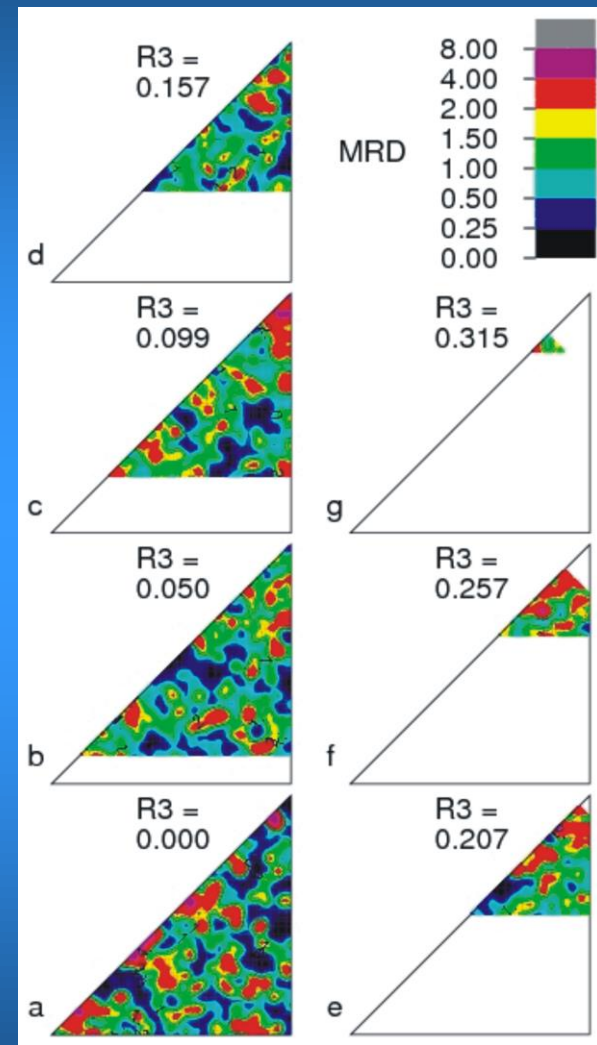
# Misorientation Distribution Functions

Rodrigues' representation  $r_1, r_2, r_3$ , cross-section  $r_3 = \text{const.}$ , asymmetric domain (O, O).  
 (High angle grain boundaries only;  $\omega > 15^\circ$ ).



Misorientation distribution between orientations of crystallites in deformation zones (before annealing) and new grains growing in the same places; 75% cold-rolled 6013 aluminum alloy

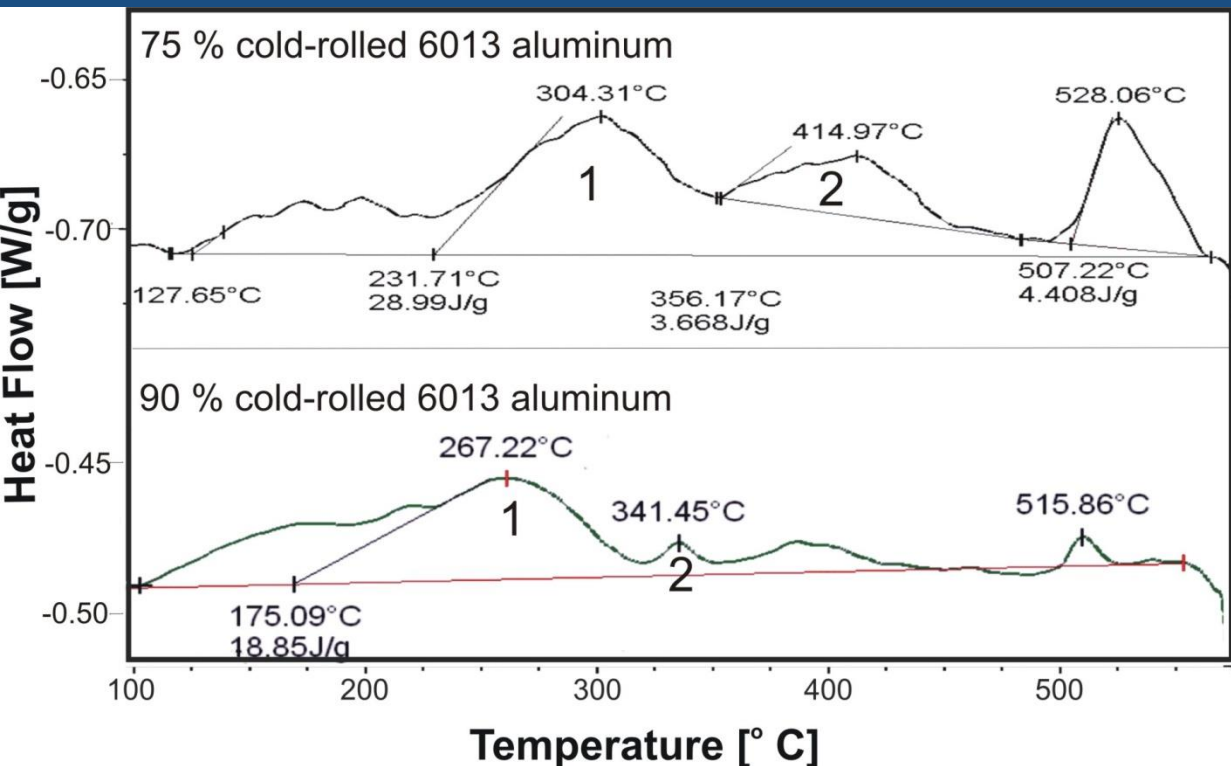
Misorientation distribution between orientations of crystallites in deformation zones (before annealing) and new grains growing in the same places; 90% cold-rolled 6013 aluminum alloy



K. Sztwiertnia

M. Bieda, K. Sztwiertnia, A. Korneva, T. Czeppe, R. Orlicki: *Orientation mapping study on the inhomogeneous microstructure evolution during annealing of 6013 aluminum alloy*, Solid State Phenomena, 16 (2010) 13-18.

# Nonisothermal annealing examination (DSC)



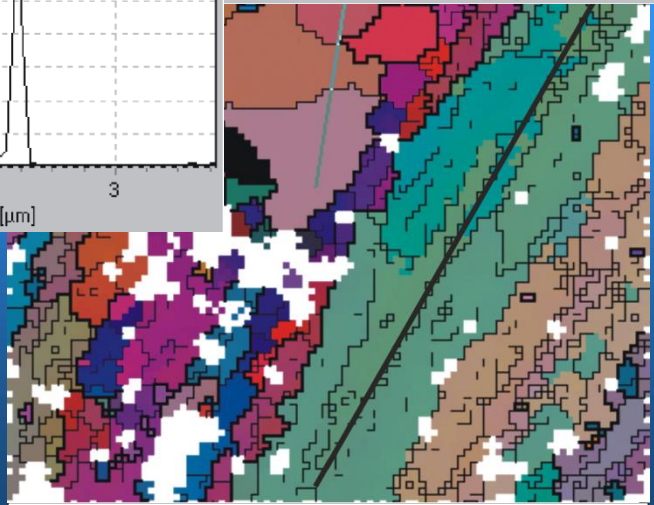
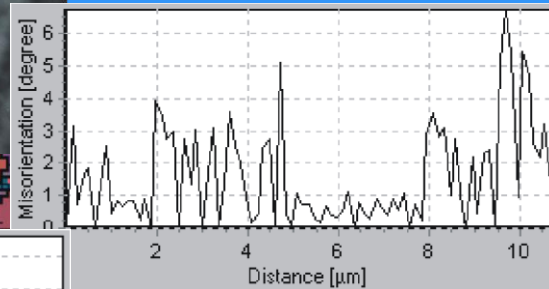
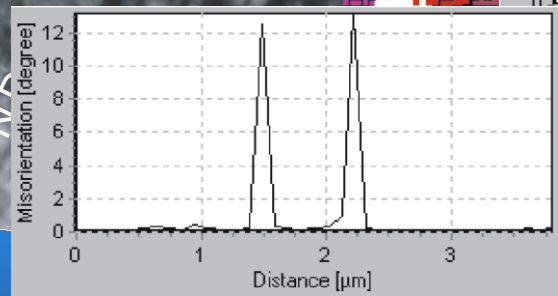
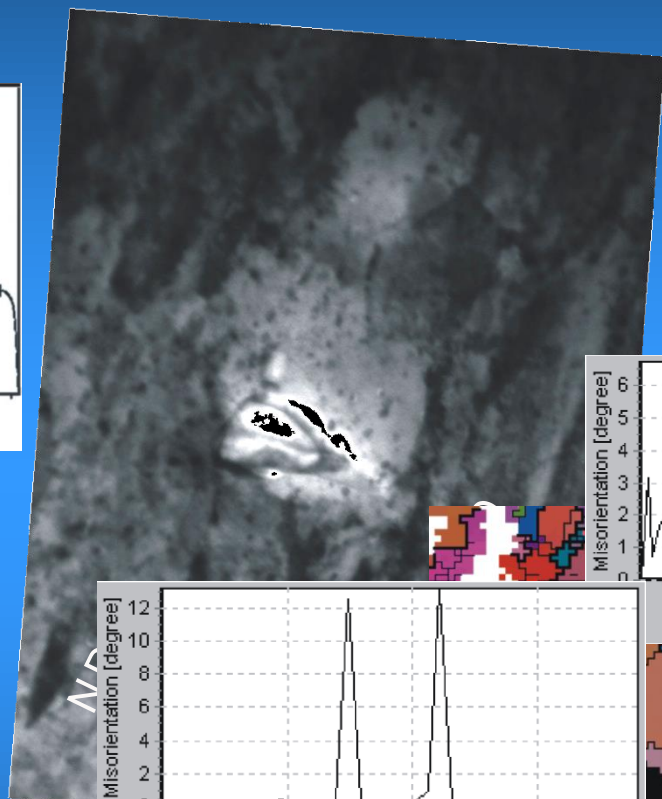
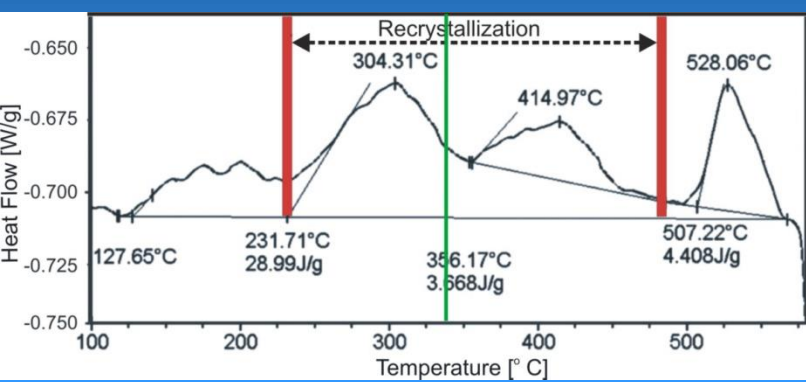
Heat flow representing the release of stored energy from 75% and 90% cold-rolled 6013 aluminum alloy.

To examine the significance of the *in situ* experiments the cold-rolled alloy samples were tested in DSC by the non-isothermal annealing method. Based on the calorimetric and microstructures studies in TEM of the appropriately in the calorimeter annealed samples, it was possible to state that the three peaks observed at the lower temperatures **were connected with the recovery and recrystallization.**

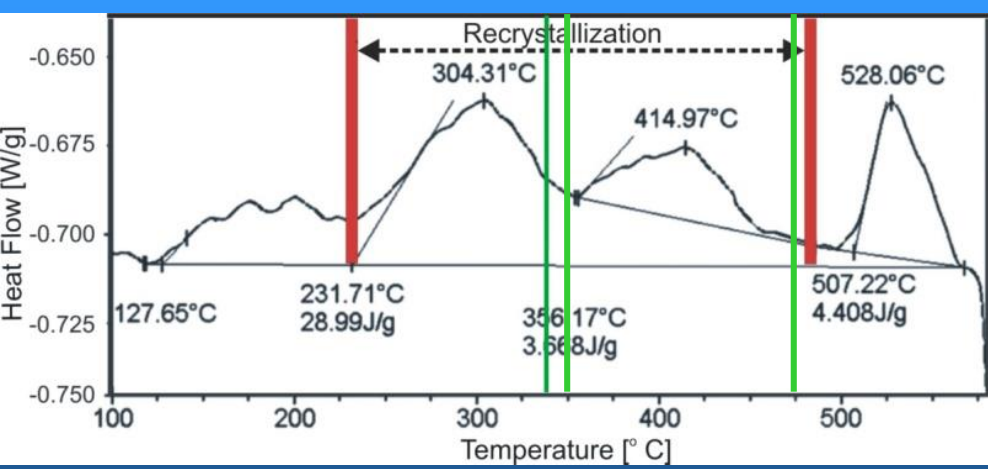
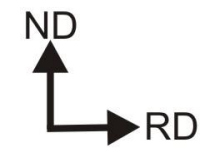
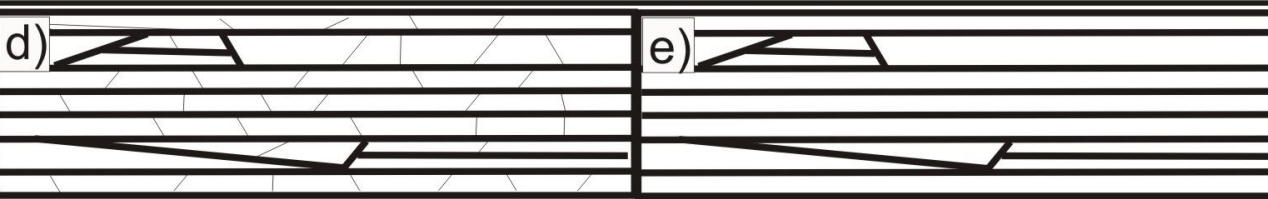
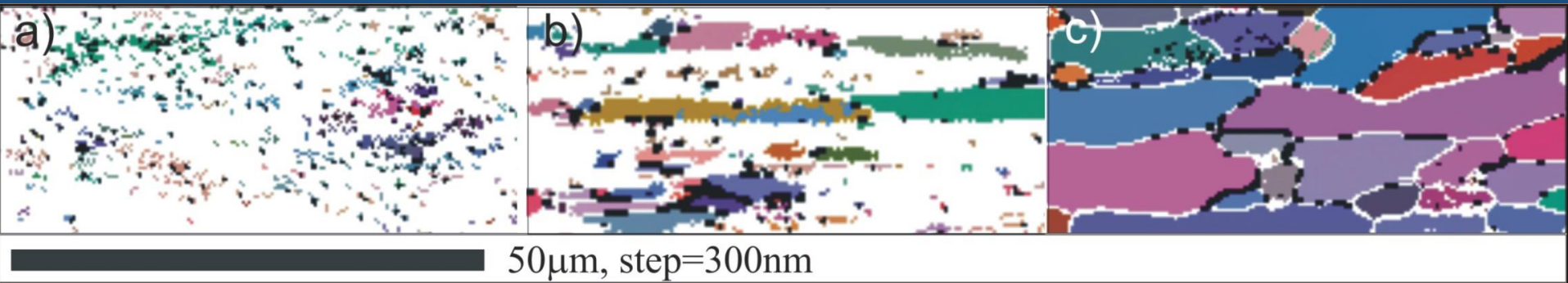
The recrystallization peaks were marked by the numbers 1 and 2.



Example of orientation topography in an area of the deformation zone around the large particle after cold rolling to 75% and heating to 330 °C in the calorimeter; 6013 aluminum alloy, longitudinal section, TEM.



# Examples of orientation topographies after cold rolling and annealing in the calorimeter; 6013 aluminum alloy, longitudinal section, EBSD/SEM/FEG.



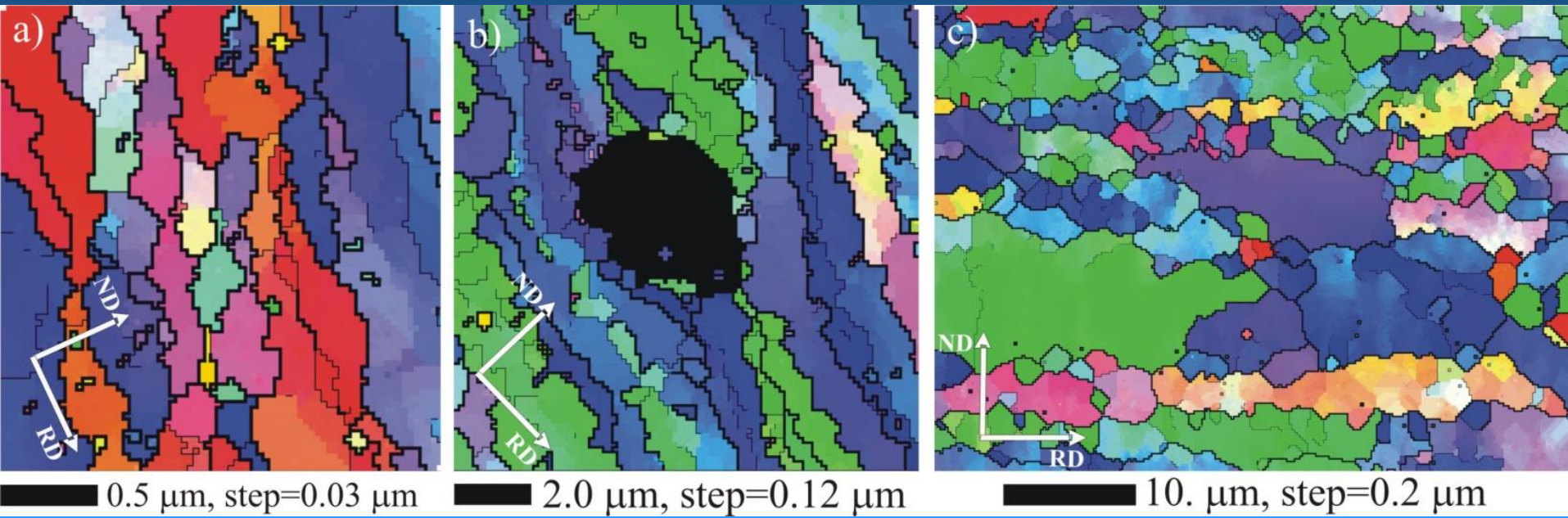
Orientation topographies of recrystallized grains in alloy 75% cold rolled and subsequently heated in the calorimeter to:

- (a) 330 °C,
- (b) 350 °C,
- (c) 480 °C.

Regions of unsolved diffractions (approximately correspond to the deformed areas) are shown in white. (d) and (e) Schematic representation of the deformed microstructure before and after annealing to the temperatures from the end of the recrystallization peak 1; thick lines – HAGBs, thin lines - LAGBs.



# Examples of orientation topographies after cold rolling and annealing in the calorimeter; 6013 aluminum alloy, longitudinal section.



Orientation topographies in samples 90% cold rolled and subsequently annealed in the calorimeter at 240  $^{\circ}\text{C}$  for 60 min:

- (a) – matrix, the total length of HAGBs  $\rightarrow$  20 - 40  $\mu\text{m}/\mu\text{m}^2$ , TEM;
- (b) – area around the large second phase particle, the total length of HAGBs  $\rightarrow$  5 - 10  $\mu\text{m}/\mu\text{m}^2$ , TEM;
- (c) – sample annealed at 380  $^{\circ}\text{C}$  for 5 min; longitudinal section, EBSD/SEM/FEG; thick lines – HAGBs  $\rightarrow$  the average length  $\sim$ 0.003  $\mu\text{m}/\mu\text{m}^2$ , thin lines – LAGBs.



## Conclusions

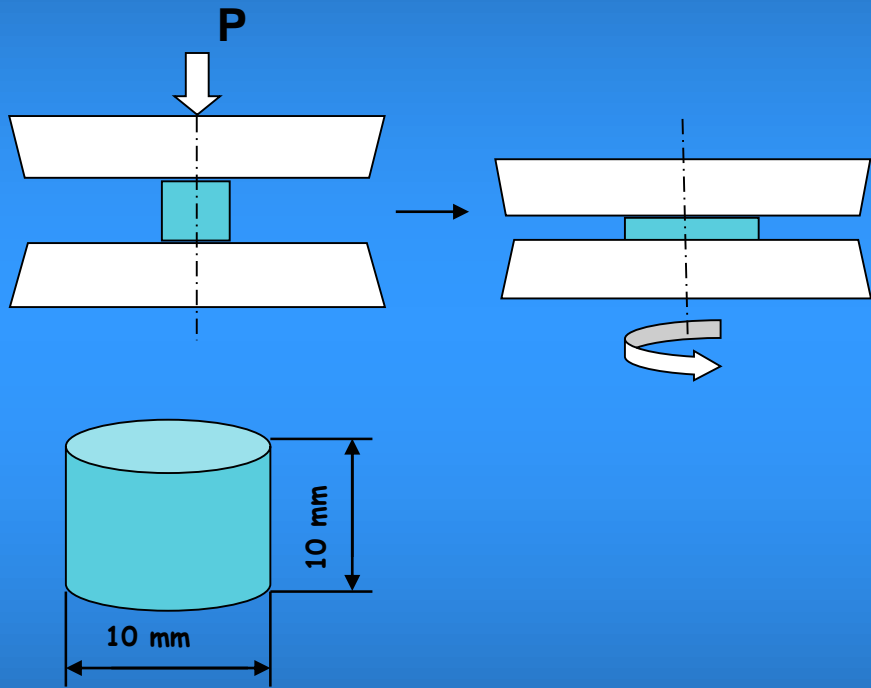
Aluminum alloy 6013, in the state after deformation, was characterized by a highly heterogeneous microstructure formed by elongated grains/subgrains almost parallel to the rolling plane and deformation zones around the large second phase particles. The distances between the HAGBs across the elongated matrix grains reached a few hundred nanometers.

The release of stored energy was separated into a few peaks, two of them were connected with the recrystallization. Due to the much higher dislocation densities in the zones, the movement of the zones HAGBs began at the lower temperatures of peak 1. The migration of the matrix HAGBs occurred only at the higher temperatures of peak 2. *It was important to distinguish the migration of HAGBs in the deformation zones from that in the matrix.*

Annealing at the temperatures below the end of recrystallization peak 1 made it possible to preserve the original laminar structure of the HAGBs in the cold-rolled matrix and to obtain microstructures with elongated grains whose thicknesses did not exceed a few hundred nanometers. This was the result of discontinuous recrystallization in the deformation zones around the large second phase particles and continuous recrystallization in the matrix. The grains were at least an order of magnitude thinner than those formed after discontinuous recrystallization occurred at the higher temperatures of peak 2.

# Example III Gradient microstructure of Fe-Cr-Co alloys subjected to complex load.

Hard magnetic Fe-Cr-Co alloys (FeCr25Co15 and FeCr30Co8) were subjected to severe plastic deformation by complex two-step loading.



Deformation temperatures:  
750, 800, 850, 900 °C

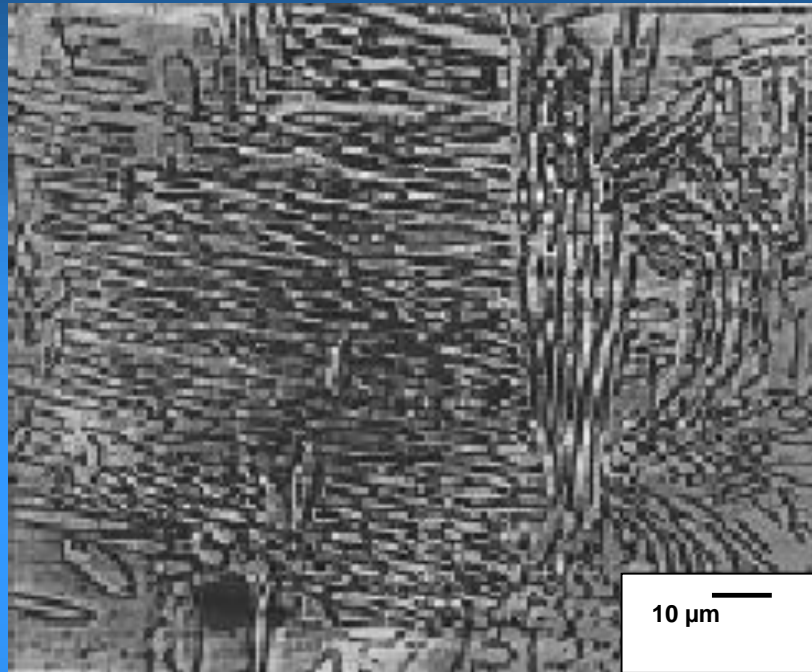
Upsetting: 40%,  $3-4 \cdot 10^{-4} \text{s}^{-1}$

Torsion: 10 rotations,  $4-8 \cdot 10^{-3} \text{s}^{-1}$

Schema of deformation by upsetting and subsequent torsion.



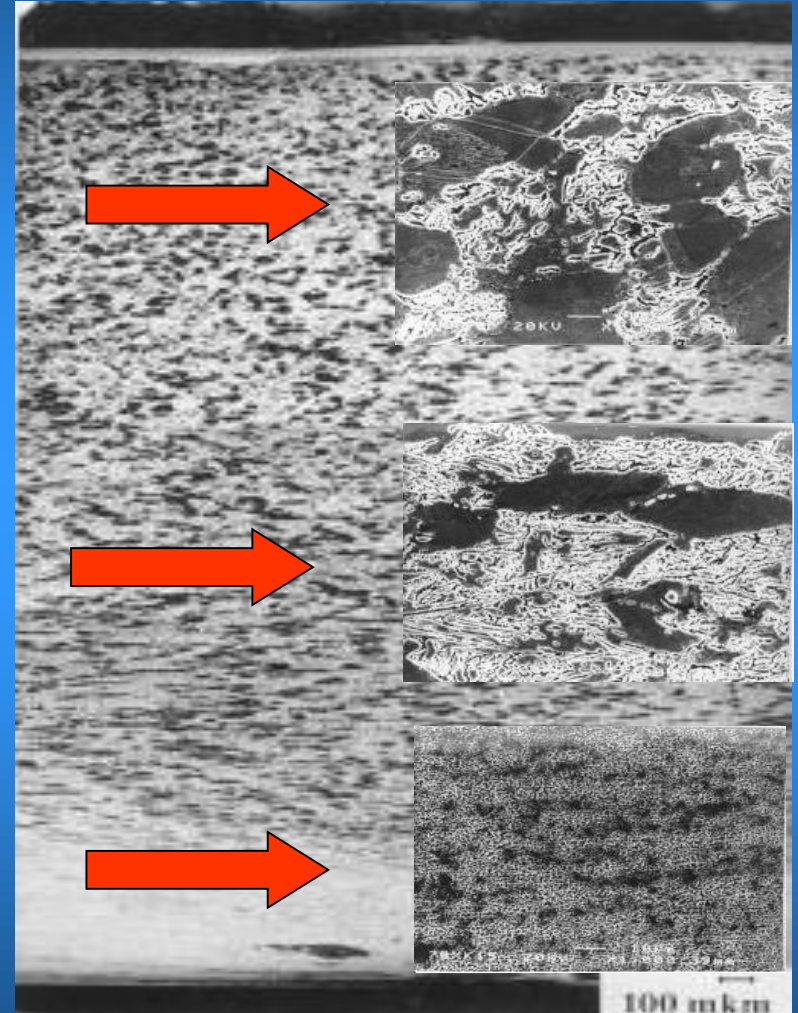
# The microstructure of the hard magnetic FeCr25Co15 alloy after deformation by two-step loading.



top part of the sample

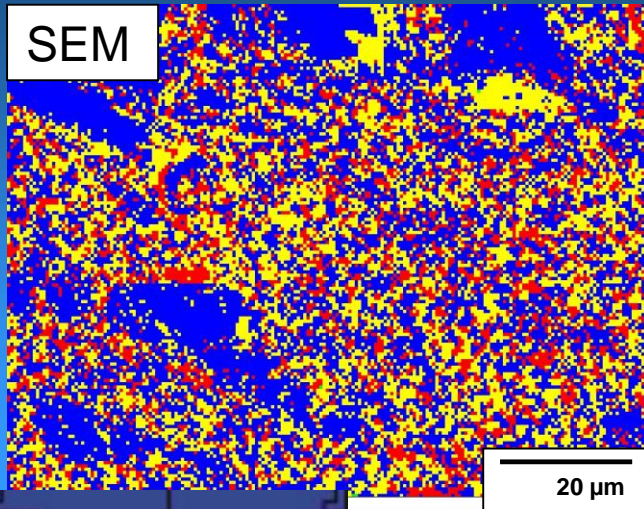
middle part of the sample

The bottom part of the sample

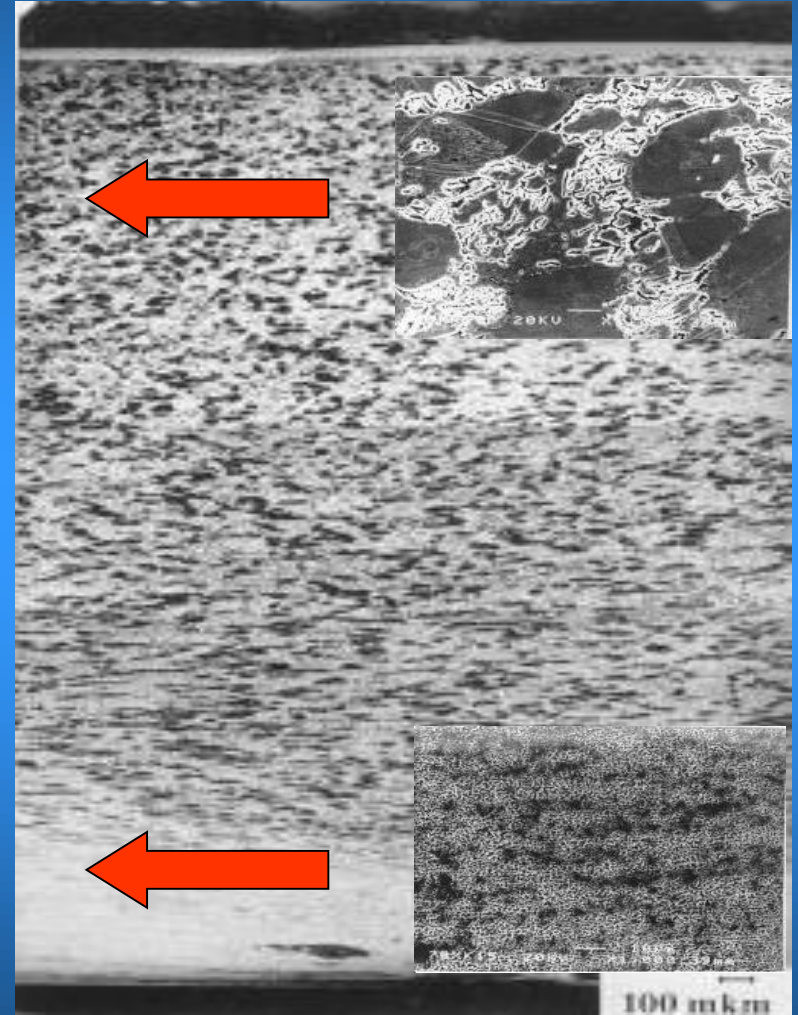
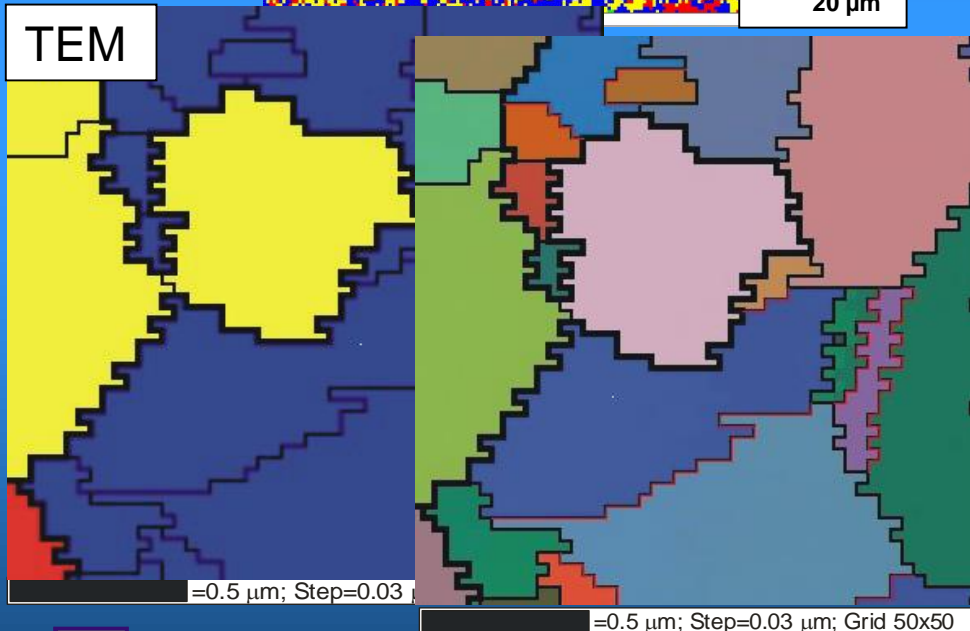




# The microstructure of the hard magnetic FeCr25Co15 alloy after deformation by two-step loading.



- γ phase
- α phase
- σ phase



K. Sztwiertnia

A.V. Korneva, M. Bieda, G.F. Korznikova and K. Sztwiertnia, Arch. Metall., 51 (2006) 69.

A.V. Korneva, M. Bieda, G.F. Korznikova and K. Sztwiertnia, Int. J. Mater. Res., in print.



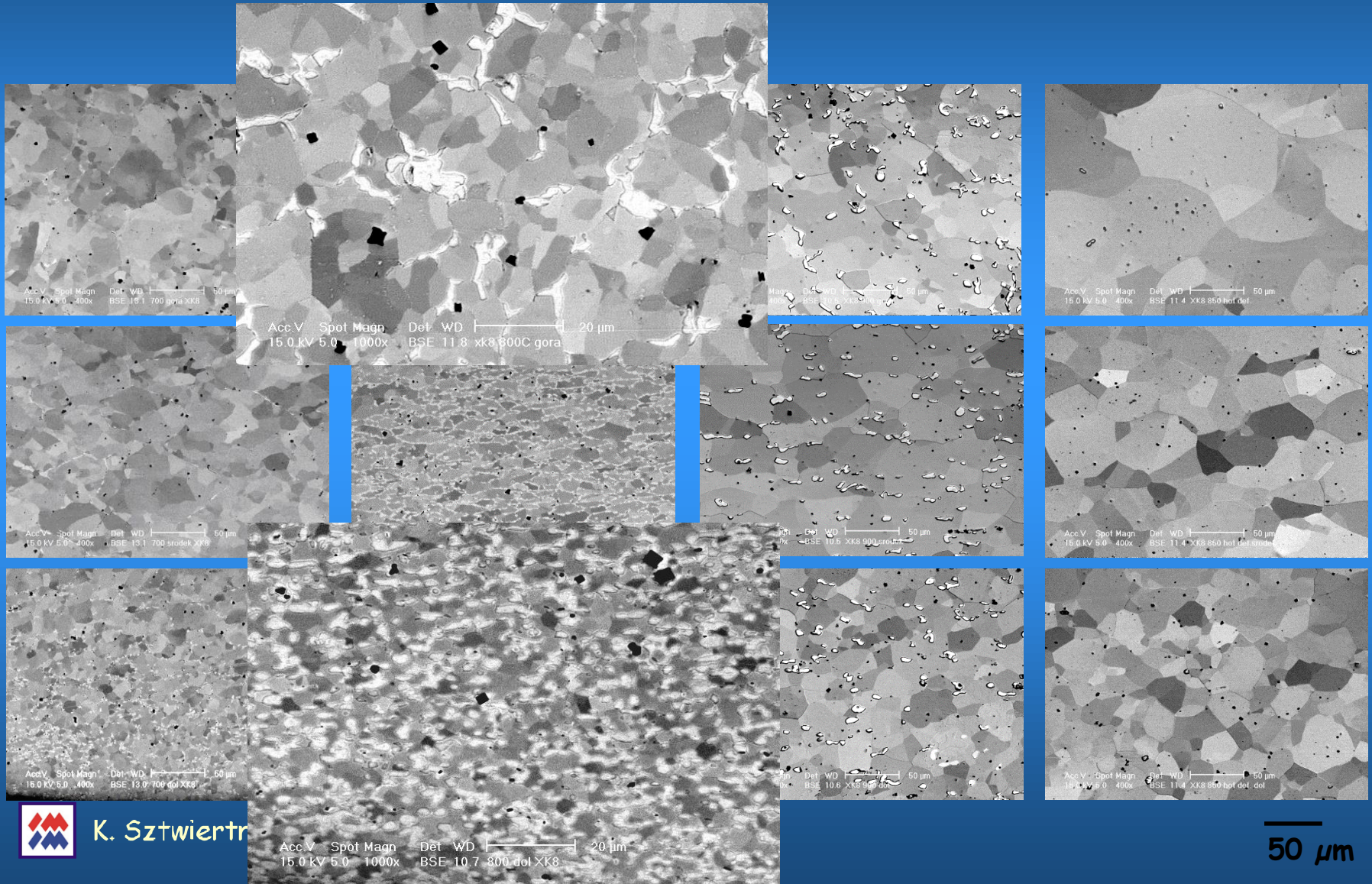
# The microstructure of the hard magnetic FeCr30Co8 alloy after deformation by two-step loading.

750 °C

800 °C

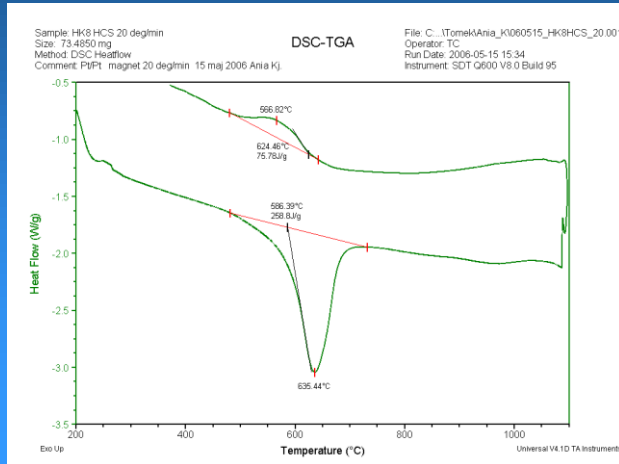
850 °C

900 °C



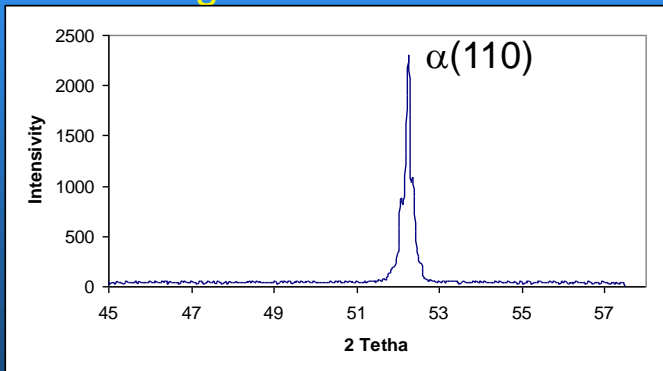
# The hard magnetic FeCr30Co8 alloy, calorimetric measurements.

FeCr30Co8, the high-coercion state.

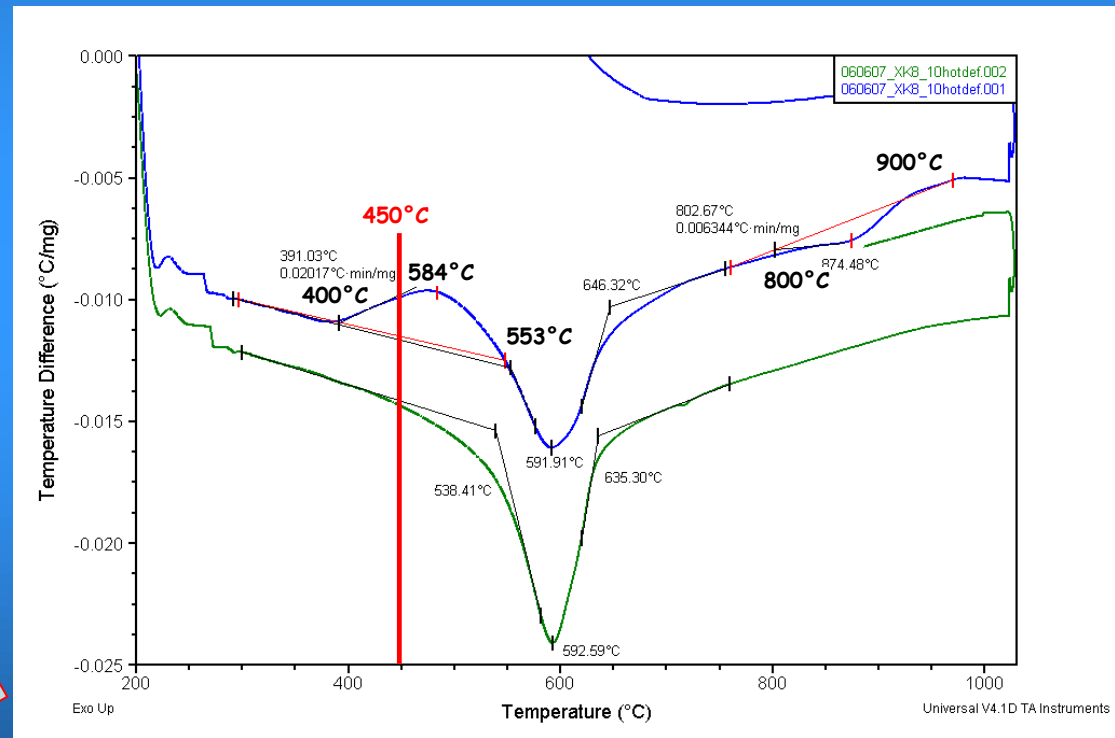


heating: 20°C/min  
cooling: 10°C/min

X-ray phase analysis after first heating in the calorimeter.

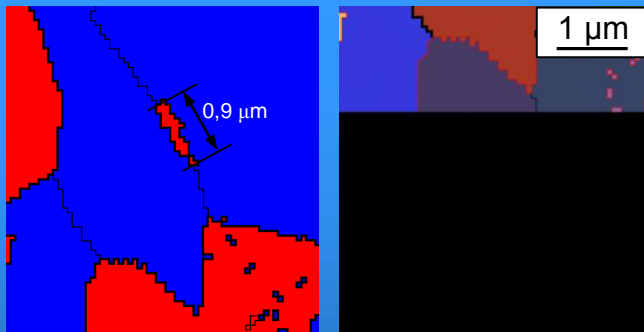
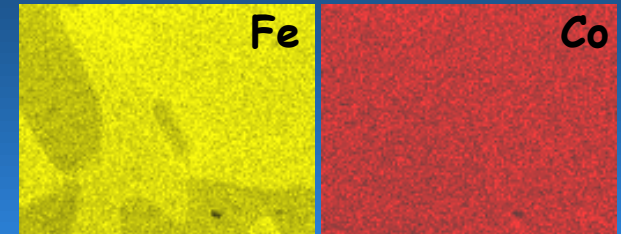
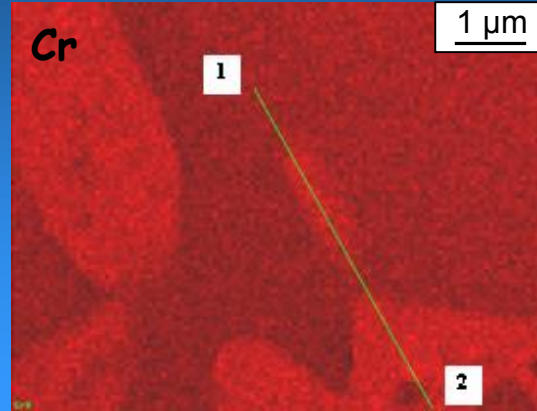
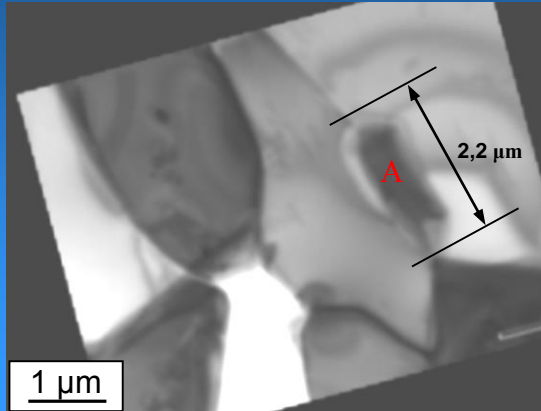


FeCr30Co8 alloy after deformation by two-step loading at the 800 °C.

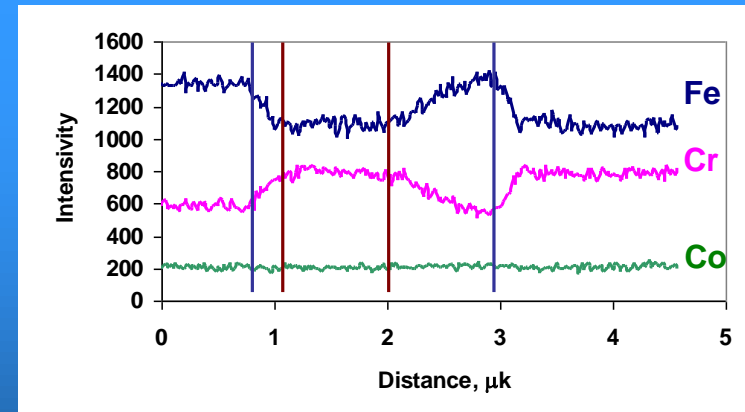


The bottom part of the sample 2x heated at the rate of 10 °C/min

# The microstructure of the hard magnetic FeCr30Co8 alloy after deformation by two-step loading, TEM, EDX/TEM, CBED/TEM.



□ a phase □ σ phase



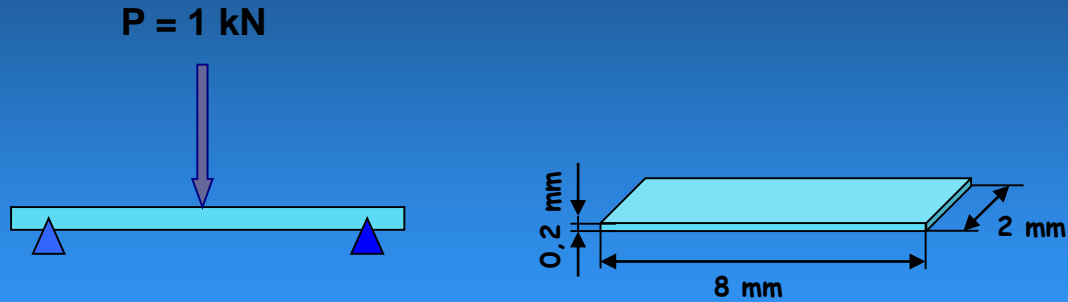
The bottom part of the sample, deformed at 800 °C and heated in the calorimeter, TEM.



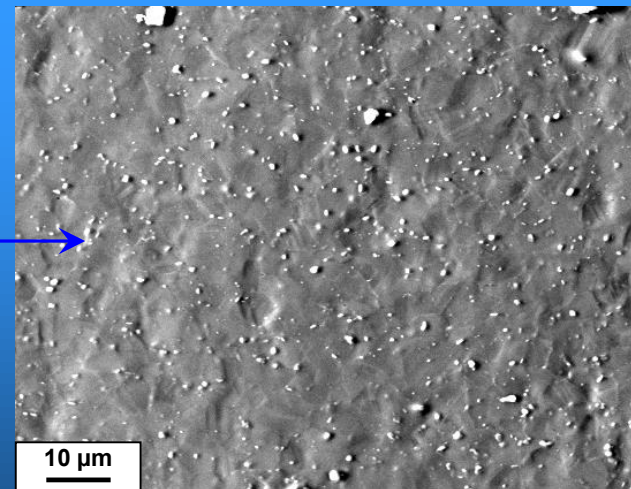
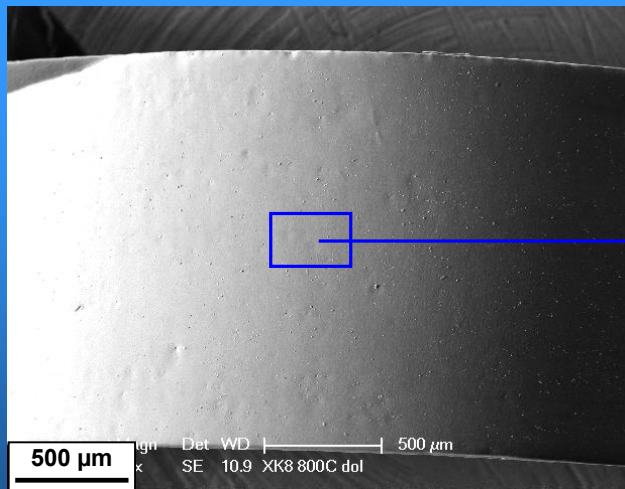
K. Sztwiertnia



# Three-point bending test of samples deformed at 700, 750, 800, 850 and 900 °C and subjected to magnetic treatment.



The surface shape after the three-point bending in the lower part of the sample (deformed at 800 °C), SEM.





## CONCLUSIONS

- The deformation of the FeCr30Co8 and FeCr25Co15 alloys by the complex load in the temperature range of 700 to 900°C results in a transformation of the lamellar microstructure into a gradient one with the minimum grain size (200 - 500 nm) in the high-deformation zone.
- The optimal temperature range for obtaining submicron-grained microstructures in the high-deformation zone is 700 to 750 °C for FeCr25Co15 and 800 °C for FeCr30Co8.
- High deformation results in the precipitation of the  $\sigma$  phase and an increased hardness of the material. Therefore, the method can be used for surface strengthening of the material, particularly when it is intended to work under friction.
- The magnetic treatment of the deformed sample results in decrease of the  $H_c$ ,  $B_r$ , and  $B_s$  values when compared to the high-coercion state. The mechanical properties of the sample are better. Increased material ductility, which should be attributed to the formation of a fine-grained microstructure and to the presence of the ductile  $\gamma$  phase, remained after magnetic treatment.
- The gradient microstructure of the material is characterised by a gradual change of the material properties. This can be advantageous in the case of magnets, which should have good magnetic properties within their volume while maintaining good mechanical properties on the surface.



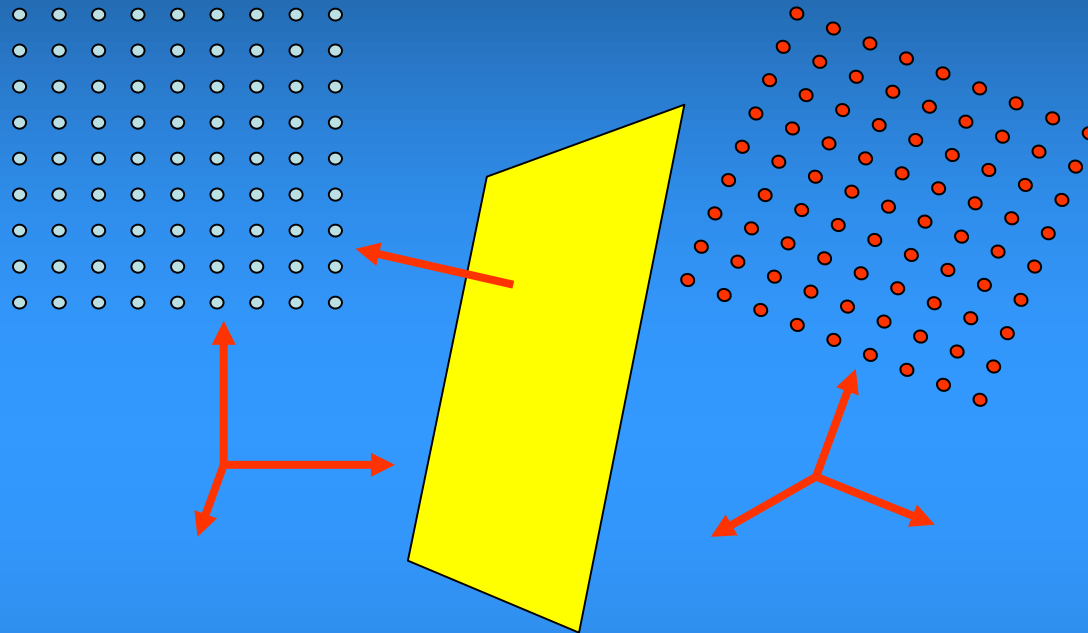
## Example II: Orientation mapping applied to composites.

# Misorientation Characteristics of Interphase Boundaries

- Misorientation in boundary description.
- Misorientation characteristic of interphase boundaries in  $\text{Al}_2\text{O}_3/\text{WC}$  composites.



# The geometry of interfaces

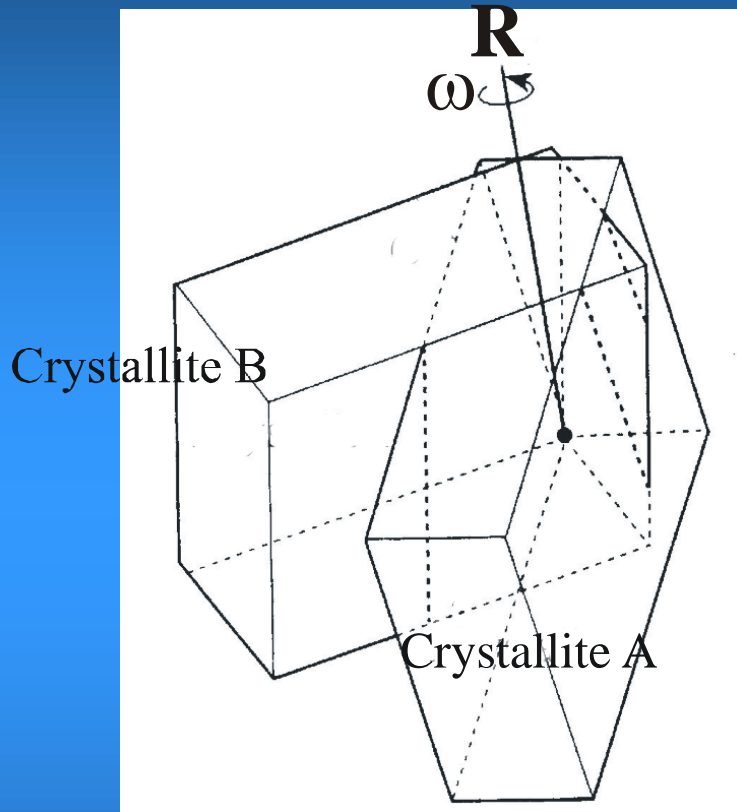


## Geometry of the grain boundary:

- ❑ The rotation between two misoriented crystal lattices (misorientation),
- ❑ The orientation of the boundary plane.



# Misorientation between two crystallites



$$K_A = \Gamma_{AB} \cdot K_B$$

$$\Gamma_{AB}^e = S_i \cdot \Gamma_{AB} \cdot P_j$$

$$(i = 1, \dots, M, j = 1, \dots, N)$$

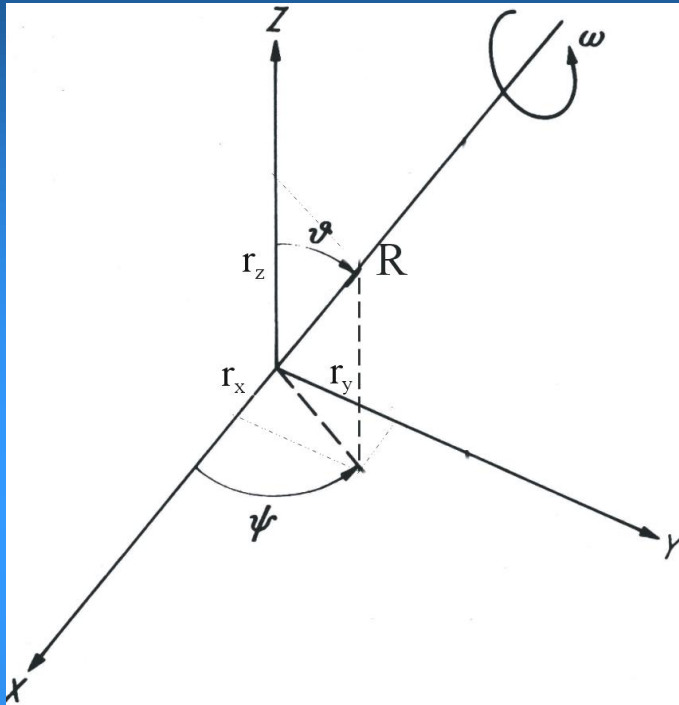
The misorientation is described by  $N \cdot M$  symmetrically equivalent variants  $\rightarrow$  for quantitative analysis of interfaces the misorientation should be made unique.

The rotation between two misoriented lattices may be described mathematically in several ways. These include the rotation matrix, the Euler angles, the axis/angle pair, the Rodrigues vector, the quaternion representation.





# Misorientation between two crystallites



Rodrigues' representation possesses certain properties of rectilinearity that make it relatively easy to construct asymmetric domains for different arrangements of crystallite symmetries.

The domains can be constructed in such a way that they contain rotations with smallest rotation angles.

The Rodrigues' parameters:

$$r_1 = r_x \cdot \operatorname{tg}(\omega/2)$$

$$r_2 = r_y \cdot \operatorname{tg}(\omega/2)$$

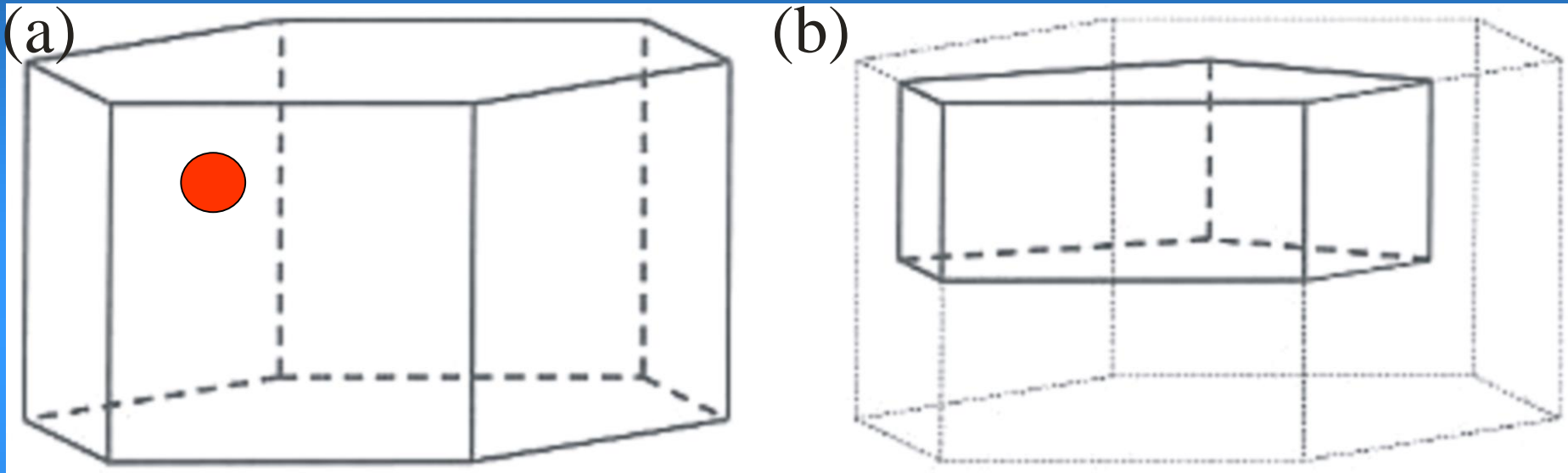
$$r_3 = r_z \cdot \operatorname{tg}(\omega/2)$$

Frank, F.C. (1987) Orientation Mapping, *Metall. Trans. A*, 19A, 403-408.



# Asymmetric domains

(Rodrigues' representation)



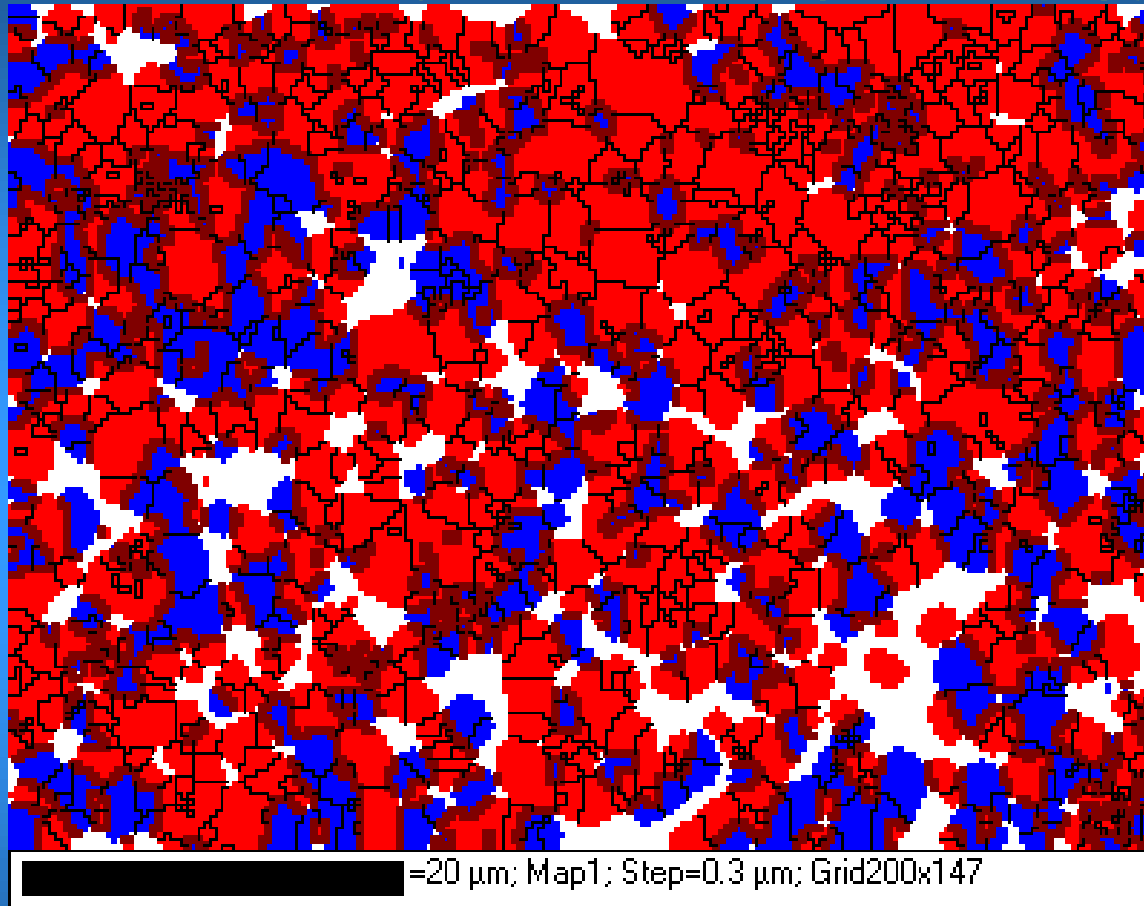
Schematic representation of the asymmetric domains for  $(D_3, C_1)$  (a) and  $(D_3, D_3)$  (b).

$$r_1, r_2, r_3 \rightarrow \begin{array}{l} (h_A \ k_A \ l_A) \parallel (h_B \ k_B \ l_B) \\ [u_A \ v_A \ w_A] \parallel [u_B \ v_B \ w_B] \end{array}$$

Morawiec, A. (2003) *Orientations and Rotations*, Springer Verlag, Berlin.



## Microstructure of Al<sub>2</sub>O<sub>3</sub>/ WC composite (ESEM/EBSD phase map)



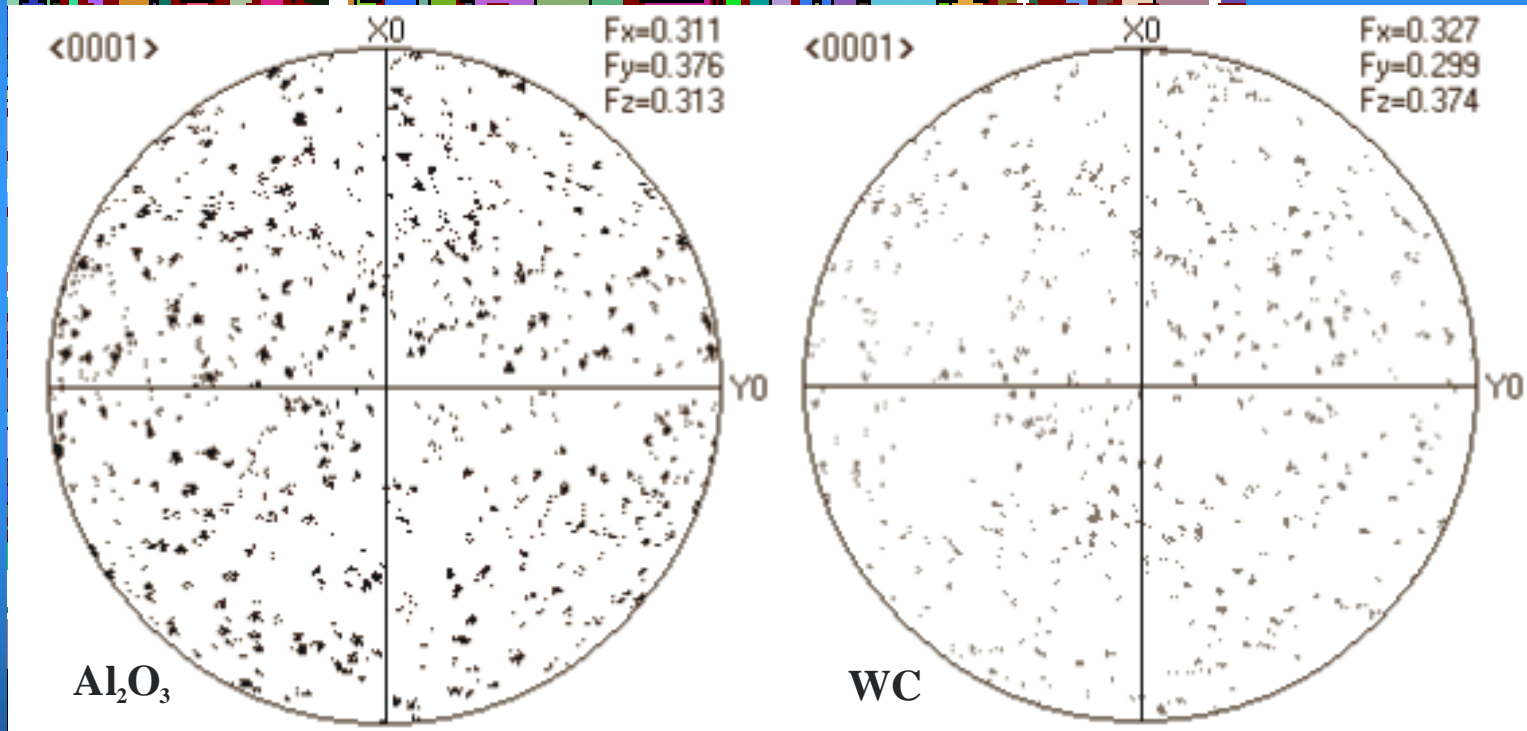
Al<sub>2</sub>O<sub>3</sub> grains – red, WC grains – blue, white regions – not indexed; thick lines – Al<sub>2</sub>O<sub>3</sub>/WC interphase boundaries, thin lines – grain boundaries.



K. Sztwiertnia

K. Sztwiertnia, M. Faryna, G. Sawina, J. Eur. Ceram. Soc., 26 (2006) 2973.

# Microstructure of $\text{Al}_2\text{O}_3$ / WC composite (ESEM/EBSD orientation map)



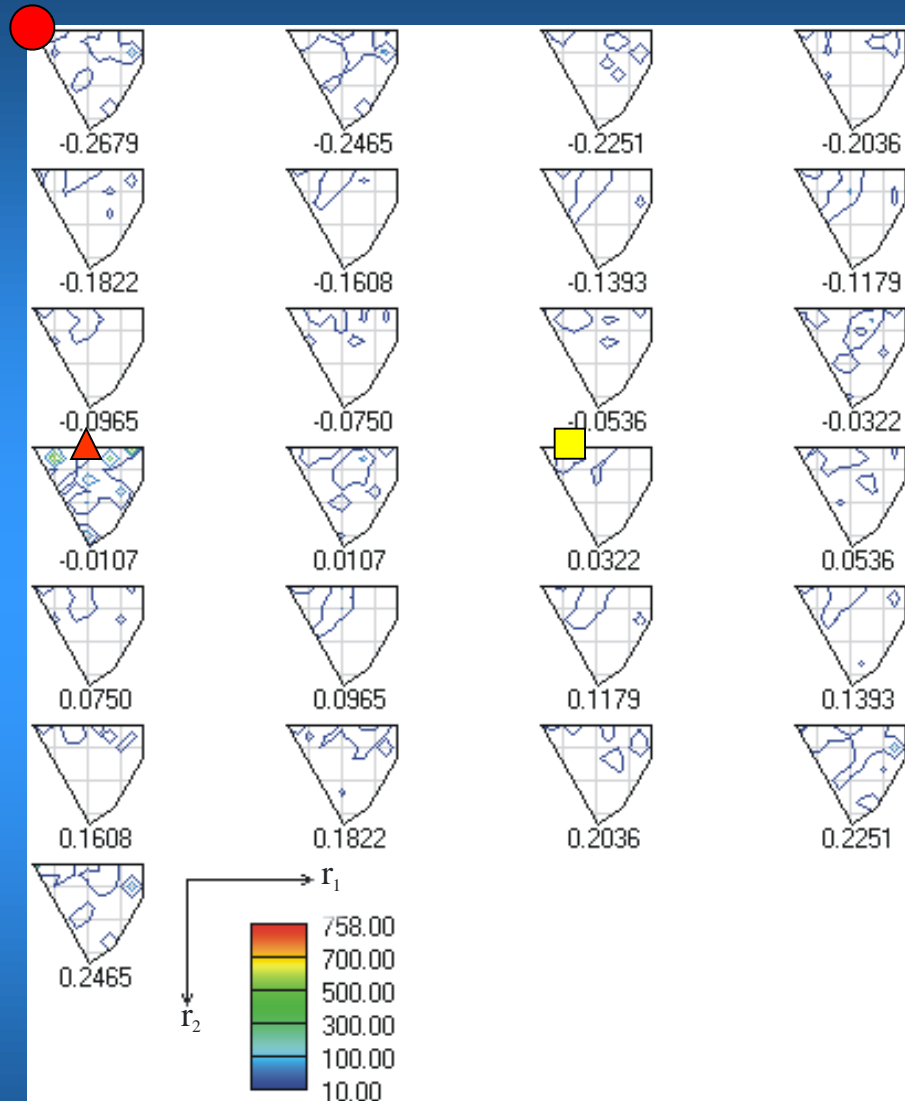
K. Sztwiertnia


Stereographic projections of directions  $\langle 0001 \rangle$  in  $\text{Al}_2\text{O}_3$  grains and WC grains, respectively.

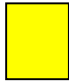
K. Sztwiertnia, M. Faryna, G. Sawina, J. Eur. Ceram. Soc., 26 (2006) 2973.




# Misorientation Distribution Function ( $Al_2O_3/WC$ )




 $(0\bar{1}11) WC \parallel (1\bar{1}05) Al_2O_3$   
 $[11\bar{2}3] WC \parallel [\bar{2}3\bar{1}1] Al_2O_3$

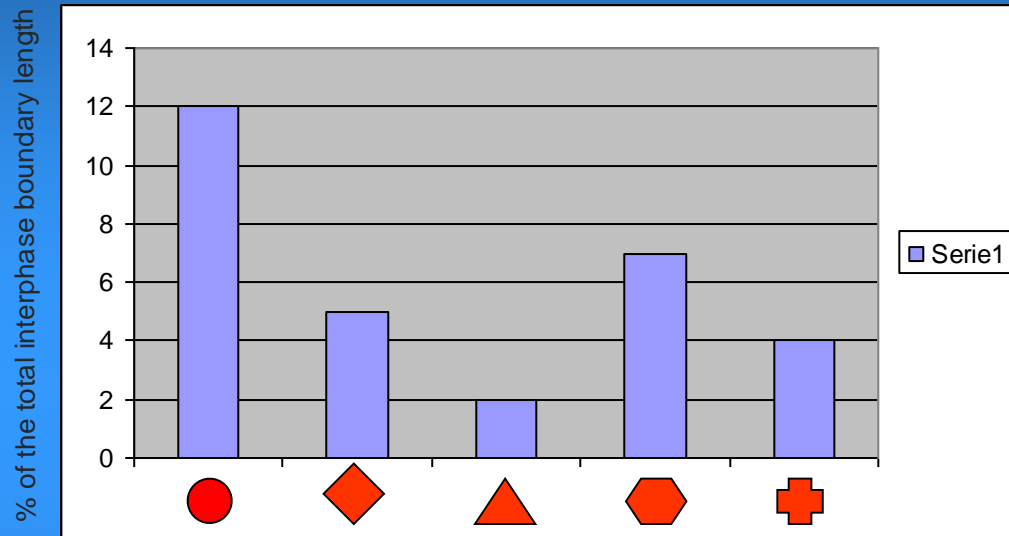

 $(0\bar{1}11) WC \parallel (\bar{1}011) Al_2O_3$   
 $[2\bar{1}\bar{1}0] WC \parallel [01\bar{1}1] Al_2O_3$


 $(0001) WC \parallel (0001) Al_2O_3$   
 $[11\bar{2}0] WC \parallel [10\bar{1}0] Al_2O_3$






MDF between  $Al_2O_3$  and WC grains;  
 Rodrigues' representation  $r_1, r_2, r_3$ ,  
 cross-section  $r_3=const.$ , asymmetric  
 domain ( $D_6, D_3$ ).



# Misorientation Distribution Function ( $Al_2O_3/WC$ )



The crystallographic relationships correspond respectively to: 12%, 5%, 2%, 7% and 4% of the total  $WC/Al_2O_3$  interphase boundary length.

- 
 $(0001) WC \parallel (0001) Al_2O_3$   
 $[11\bar{2}0] WC \parallel [10\bar{1}0] Al_2O_3$
- 
 $(10\bar{1}0) WC \parallel (10\bar{1}0) Al_2O_3$   
 $[000\bar{1}] WC \parallel [\bar{1}3\bar{2}\bar{2}] Al_2O_3$
- 
 $(10\bar{1}0) WC \parallel (10\bar{1}0) Al_2O_3$   
 $[000\bar{1}] WC \parallel [\bar{4}9\bar{5}2] Al_2O_3$
- 
 $(2\bar{1}\bar{1}0) WC \parallel (2\bar{1}\bar{1}0) Al_2O_3$   
 $[000\bar{1}] WC \parallel [01\bar{1}0] Al_2O_3$
- 
 $(3\bar{1}\bar{2}0) WC \parallel (3\bar{1}\bar{2}0) Al_2O_3$   
 $[01\bar{1}\bar{1}\bar{2}] WC \parallel [\bar{1}9\bar{8}\bar{1}] Al_2O_3$



thank you